AD-A068 002 OKLAHOMA UNIV NORMAN SCHOOL OF AEROSPACE MECHANICAL --ETC F/G 20/4
HYPERSONIC FLOW PAST A SLENDER ELLIPTIC CONE.(U)
NOV 78 H M LEE, M L RASMUSSEN AFOSR-77-3468
UNCLASSIFIED OU-AMNE-78-2 AFOSR-TR-79-0473 NL

| OF |
AD
A068002

END
DATE
FILMED
6-79
DDC

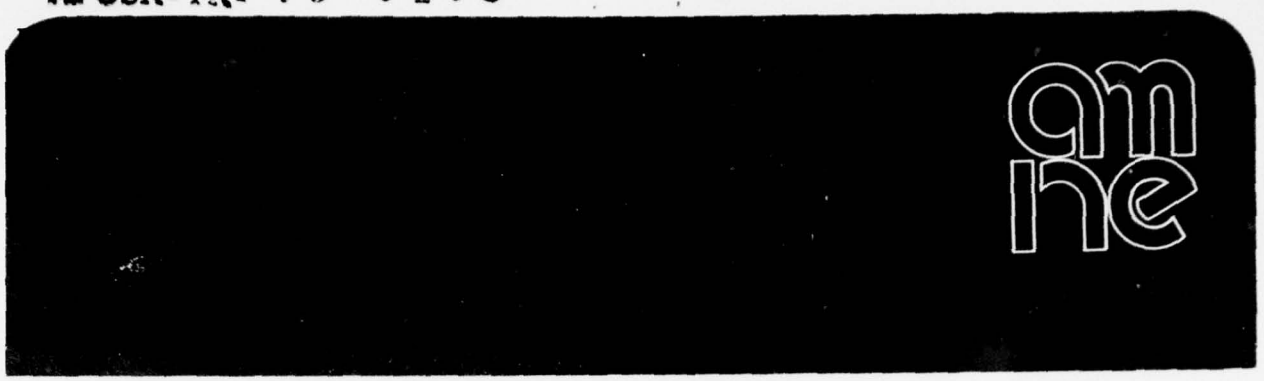

LEVEL II

University of Oklahoma
School of Aerospace, Mechanical and Nuclear Engineering
Research Report No. OU-AMNE 78-2

HYPERSONIC FLOW PAST A SLENDER ELLIPTIC CONE

by

Hsiung Ming Lee
and
Maurice L. Rasmussen

Prepared for
USAF Office of Scientific Research under
Grant AFOSR 77-3468
OU ORA 158-005
November 1978

ABSTRACT

An approximate analytical solution is obtained for hypersonic flow past a slender elliptic cone at small angle of attack. The analysis is based on perturbations of hypersonic flow past a circular cone aligned with the free stream, the perturbations stemming from the linear combination of small angle of attack and small cross-section eccentricity. By means of previously obtained hypersonic approximations for the basic-cone problem, closed-form approximate solutions for the perturbation equations are obtained within the framework of hypersonic small-disturbance theory. Results for the shock shape, shock-layer structure, and surface conditions are presented, together with comparisons with experimental data.

ACKNOWLEDGEMENTS

This investigation was sponsored by the United States Air Force, Office of Scientific Research, under Grant No. AFOSR 77-3468. This report is a slightly modified version of the Master of Science thesis by Mr. Hsiung Ming Lee. The authors thank Professor Martin Jischke for numerous valuable discussions. Thanks go also to our project monitor, Dr. Donald Daniel, for his encouragement and comments.

TABLE OF CONTENTS

ACKNOWLEDGEMENTS iii

LIST OF ILLUSTRATIONS vi

LIST OF SYMBOLS vii

1. INTRODUCTION 1

2. UNYAWED ELLIPTIC CONE BODY AND SHOCK GEOMETRY 4

   2.1 Body Geometry 4

   2.2 Shock Geometry 7

3. BOUNDARY CONDITIONS 9

   3.1 Expansions for the Flow Variables 9

   3.2 Free Stream Normal Velocity at the Shock 9

   3.3 Downstream Pressure at the Shock 10

   3.4 Downstream Density at the Shock 11

   3.5 Downstream Velocity at the Shock 11

4. PERTURBATION EQUATIONS 14

   4.1 Energy Equation 14

   4.2 Momentum Equation 16

   4.3 Continuity Equation 18

5. APPROXIMATE SOLUTION FOR HYPERSONIC FLOW 23

   5.1 Basic Cone-Flow Approximations. 23

   5.2 Evaluations of Integrals 23

   5.3 Approximation for the Velocity 24

   5.4 Shock Eccentricity Factor 26

   5.5 Shock-Layer Velocity Profiles 27

   5.6 Evaluation of the Approximate Analysis. 33

6. SURFACE PRESSURE ON THE ELLIPTIC CONE. 38

   6.1 Surface Perturbation Pressure Coefficient 38

   6.2 Comparison with Experiment. 41

   6.3 Drag on the Elliptic Cone 43

7. ELLIPTIC CONE AT ANGLE OF ATTACK 47

   7.1 Superposition of Results 47

   7.2 Pressure on the Body Surface. 48

   7.3 Comparison with Other Results 49

   7.4 Normal Force on the Elliptic Cone 54

8. CONCLUDING REMARKS 56

REFERENCES 57

LIST OF ILLUSTRATIONS

Figure		Page
2.1	Cone Coordinates and Geometry	5
2.2	Two-Term Fourier Representation of the Ellipse	8
5.1	Elliptic-Cone Shock Eccentricity Factor, $\gamma = 1.4$	28
5.2	Radial Perturbation Velocity, $\gamma = 1.4$	29
5.3	Polar Perturbation Velocity Components, $\gamma = 1.4$	30
5.4	Azimuthal Perturbation Velocity Component, $\gamma = 1.4$	31
5.5	Azimuthal Velocity at the Body Surface, $\gamma = 1.4$	32
5.6	Correction Velocity Ratio, $\gamma = 1.4$	36
6.1	Perturbation Pressure Coefficient on the Body Surface	40
6.2	Pressure Coefficient on Body Surface, Model I, $M_\infty = 6$, $\gamma = 1.4$	44
6.3	Pressure Coefficient on Body Surface, Model II, $M_\infty = 6$, $\gamma = 1.4$	44
6.4	Pressure Coefficient on Body Surface, Model I, $M_\infty = 3.09$, $\gamma = 1.4$	45
6.5	Pressure Coefficient on Body Surface, Model II, $M_\infty = 3.09$, $\gamma = 1.4$	45
7.1	Angle-of-Attack Perturbation Surface Pressure Coefficient $\gamma = 1.4$	50
7.2	Comparison of Surface Pressure with Martellucci's Results, Model I, $M_\infty = 6$, $\gamma = 1.4$	52
7.3	Comparison of Surface Pressure with Martellucci's Results, Model II, $M_\infty = 6$, $\gamma = 1.4$	53

LIST OF SYMBOLS

a	tangent of semivertex angle of semiminor axis
a_o	zeroth order isentropic speed of sound
A	basic area of finite cone
b	tangent of semivertex angle of semimajor axis
C_M	moment coefficient
C_N	normal force coefficient
c_v	constant density specific heat
$\underset{\sim}{c}_p$	surface pressure coefficient
C_p	surface pressure coefficient associated with angle of attack
D	drag force
e	eccentricity of elliptic cone
$\vec{F}$	force on finite cone
F_1	constant, see Equation (4.10)
$\underset{\sim}{F}_1$	constant, see Equation (7.6)
f_1	constant, see Equation (5.10)
g	shock eccentricity factor associated with elliptic cone
$\underset{\sim}{g}$	shock eccentricity factor associated with angle of attack
$H_o(\theta)$	function, see Equation (4.32a)
$H_1(\theta)$	function, see Equation (4.32b)
$I(\theta)$	function of integration, see Equation (4.22)
K_s	hypersonic similarity parameter
M	Mach number
$\vec{M}$	moment about the cone vertex
N	constant, see Equation (5.24)

$\hat{n}$ unit normal vector

p pressure

$\tilde{p}$ pressure associated with angle of attack

r spherical coordinate

s entropy

T temperature

u,v,w spherical velocity components

$\tilde{u},\tilde{v},\tilde{w}$ spherical velocity components associated with angle of attack

V velocity

$X(\theta)$ function, see Equation (4.33)

x,y,z Cartesian coordinate

Greek Letters

α angle of attack

β unperturbed shock angle

γ ratio of specific heats

δ semivertex angle of basic circular cone

ε measure of eccentricity

θ,ϕ spherical coordinates

ξ $\rho_\infty/\rho(\beta)$, density ratio across the shock

ρ density

σ β/δ

$\vec{\Omega}$ vorticity

Subscripts

∞	free stream condition
s	condition just downstream of shock
0	zeroth order
1	first order
α	α-derivative

APPROXIMATION FOR HYPERSONIC FLOW PAST AN ELLIPTIC CONE

1. INTRODUCTION

For supersonic flows past bodies without axial symmetry, the elliptic cone is a basic body shape. Its counterpart, the circular cone, is a basic axisymmetric body shape with flow field properties that are extensively tabulated. Even the supersonic flow past a circular cone at small angle of attack is extensively tabulated and fairly well understood. On the other hand, the properties of the supersonic flow field past an elliptic cone are not extensively tabulated, at least in comparison with the circular cone at angle of attack. Although numerous papers have been directed towards supersonic flows past elliptic cones, their goals have been specific, and no general or comprehensive flow field calculations have been set forth. The purpose of this work is to partially remedy this situation and to present an approximate analytic solution that illustrates the general flow field features of hypersonic flow past a slender elliptic cone with small eccentricity.

Supersonic flow past slender cones with arbitrary cross section can be treated with some generality by means of linearized theory [1], and linearized theory can be extended to second order [2] to account somewhat for weak nonlinear effects. These results, however, are frequently not appropriate for the hypersonic Mach numbers and flow deflections of practical concern.

Another approach to the problem deals with flows that deviate slightly from the basic axisymmetric flow past a circular cone. The so-called

scheme of linearized characteristics was applied by Ferri, Ness, and Kaplita [3] to several conical bodies with non-axisymmetric cross sections. This method is subject to a number of criticisms for cross-section areas that deviate significantly from circles [4], and thus a modification of the linearized characteristics method was applied to elliptic cones at angle of attack by Martellucci [5]. In the above use of the linearized characteristics method, the perturbation equations were solved numerically. Chapkis [6], applying the linearized characteristics method, used hypersonic approximations for the basic cone flow to obtain relatively simple specific results for an elliptic cone.

Besides the above methods of computation, there are numerical schemes for integrating the complete governing gas dynamic equations. Two notable schemes applied to elliptic cones are those of Stocker and Mauger [7] and Babenko et al.[8]. There are also semi-empirical methods for dealing with certain features of supersonic flows past elliptic cones, such as tangent-cone methods, equivalent circular-cone methods, and the method of Kaattari [9]. Whichever method has been utilized to date, the general features of the supersonic flow field past an elliptic cone, showing effects of Mach number, cone angle, and ellipse eccentricity on the shock shape, the shock-layer structure, and the surface conditions, have not been delineated.

In this undertaking, we wish to start with the small-perturbation equations for perturbed flow past a basic circular cone at zero angle of attack and take the approach of Chapkis [6] for the elliptic cone. We shall use improved approximations for the basic cone flow [10,11] and obtain approximate analytical solutions for the perturbation equations. The analysis is analogous to that of Doty [12] and Doty and Rasmussen [13] for obtaining approximations for hypersonic flow past circular cones at

small angle of attack, which were shown to be very accurate. The analysis is cast in the form of hypersonic similarity theory, and the results are presented in appropriate similarity form.

The perturbation expansions involve a small parameter for the angle of attack and for the measure of the eccentricity of the ellipse cross section. These expansions are not uniformly valid in a thin vortical layer adjacent to the cone surface. It can be shown [14,15], however, that at least the pressure and azimuthal velocity component are valid across the vortical layer. Since these two variables are of most importance, further consideration of the vortical layer will not be undertaken.

2. UNYAWED ELLIPTIC CONE BODY AND SHOCK GEOMETRY

2.1 Body Geometry

In rectangular Cartesian coordinates, as shown in Fig. 2.1, the unyawed elliptic cone body is represented by

$$\frac{x^2}{a^2 z^2} + \frac{y^2}{b^2 z^2} = 1 \quad , \tag{2.1}$$

where $a \equiv \tan \theta_a$ and $b \equiv \tan \theta_b$ are the tangents of the semivertex angles of the semiminor and semimajor axes of the elliptic cone. In terms of spherical polar coordinates, also shown in Fig. 2.1, equation (2.1) can be rewritten as

$$\tan \theta = \frac{\tan \theta_m}{\sqrt{1 + e \cos 2\phi}} \tag{2.2}$$

where

$$\tan \theta_m \equiv \frac{\sqrt{2}\, ab}{\sqrt{a^2 + b^2}} = b\sqrt{1-e} = a\sqrt{1+e} = \sqrt{ab}\,(1-e^2)^{1/4} \tag{2.3a}$$

$$e \equiv \frac{b^2 - a^2}{b^2 + a^2} \tag{2.3b}$$

The parameter e is a measure of the eccentricity of the elliptic cone.

The first three terms of the Fourier-series representation of equation (2.2) are given by

$$\tan \theta = \tan \theta_m \, [A_o + A_2 \cos 2\phi + A_4 \cos 4\phi + \ldots] \quad , \tag{2.4}$$

where

$$A_o \equiv \frac{2}{\pi} \frac{K(k)}{\sqrt{1+e}} \tag{2.5a}$$

$$A_2 \equiv -\frac{4}{\pi k^2 \sqrt{1+e}} [(2-k^2)\, K(k) - 2E(k)] \tag{2.5b}$$

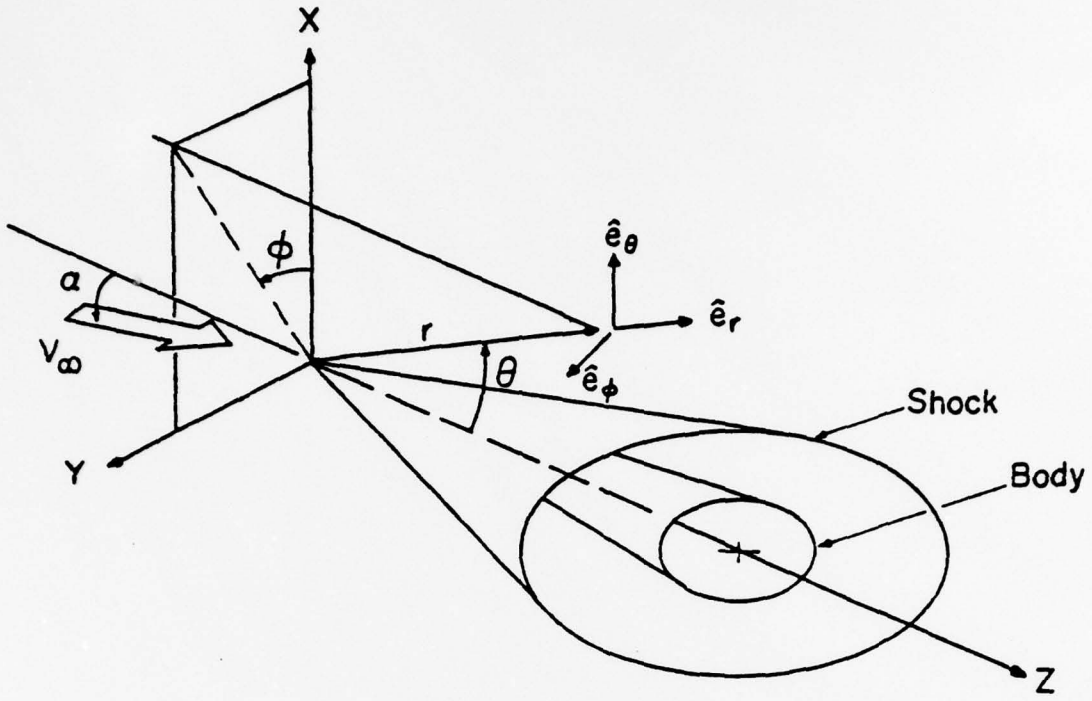

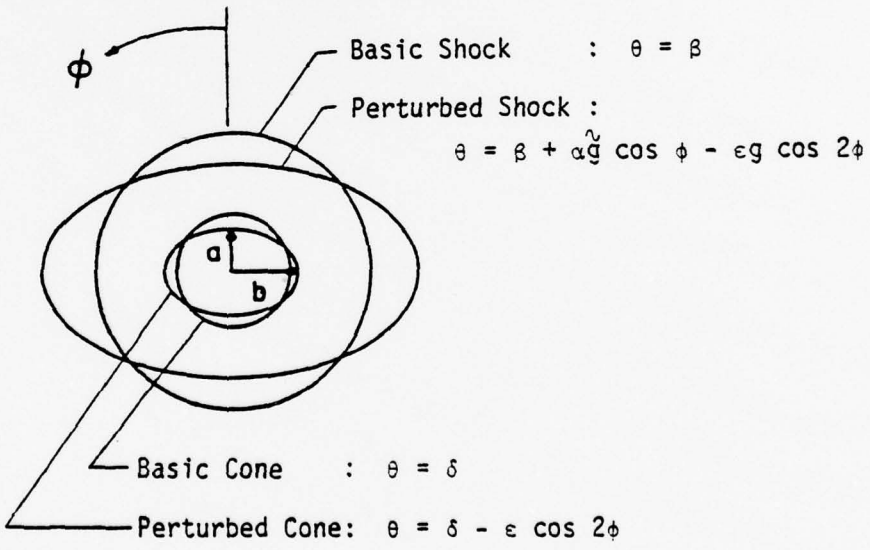

Figure 2.1 Cone Coordinates and Geometry

$$A_4 \equiv -\frac{2}{3} A_o - \frac{4}{3e} A_2 \tag{2.5c}$$

$$K^2 \equiv \frac{2e}{1+e} \tag{2.5d}$$

and

$$E(k) \equiv \int_0^{\pi/2} \sqrt{1 - k^2 \sin^2 u}\ du \tag{2.5e}$$

$$K(k) \equiv \int_0^{\pi/2} \frac{du}{\sqrt{1 - k^2 \sin^2 u}} \tag{2.5f}$$

are the complete elliptic integrals of the first and second kinds. For small values of the eccentricity, e, the Fourier coefficients can be expanded as

$$A_o = 1 + \frac{3}{16} e^2 + O(e^4) \tag{2.6a}$$

$$A_2 = -\frac{e}{2} \left[1 + \frac{15}{32} e^2 + O(e^4) \right] \tag{2.6b}$$

$$A_4 = \frac{3}{16} e^2 \left[1 + \frac{35}{48} e^2 + O(e^4) \right] \tag{2.6c}$$

When the eccentricity, e, is small the successive Fourier coefficients become smaller and smaller. For sufficiently small e, the Fourier coefficients for the higher harmonics can be neglected.

We can expand equation (2.4) for θ in a Fourier expansion and obtain for small eccentricities

$$\theta = \delta - \varepsilon \cos 2\phi + O(\varepsilon^2) \tag{2.7}$$

where

$$\delta \equiv \tan^{-1}(A_o \tan \theta_m) - \frac{A_o A_2^2}{4} \sin 2\theta_m + O(e^4)$$

$$\equiv \theta_m + \frac{e^2}{32} [3 - 2\sin^2\theta_m] \sin 2\theta_m + O(e^4) \tag{2.8a}$$

$$\varepsilon \equiv -\frac{A_2 \tan \theta_m}{1 + A_o^2 \tan^2 \theta_m} \left[1 - \left(\frac{A_2^2}{4} + A_4\right) \sin^2\theta_m + \frac{A_2^2}{4} (1 + 3A_o^2) \sin^4\theta_m + O(e^4)\right]$$

$$\varepsilon \equiv \frac{e}{4}\left[1 + e^2\left\{\frac{15}{32} - \frac{5}{8}\sin^2\theta_m + \frac{1}{4}\sin^4\theta_m\right\} + O(e^4)\right]\sin 2\,\theta_m \qquad (2.8b)$$

The parameter ε is a new measure of the eccentricity and is the appropriate parameter to be used in the subsequent analysis. The parameter δ specifies the semivertex angle of the basic circular cone about which a perturbation analysis is to be performed.

Comparison of the two-term approximation (2.7) with the exact equation (2.2) for the elliptic cone is shown in Fig. 2.2. When a = 0.2555 and b = 0.3562, such that e = 0.320 and $\theta_m = 16.30°$, the two-term approximation gives a good representation of the actual ellipse. When a = 0.2256 and b = 0.4034, such that e = 0.523 and $\theta_m = 15.56°$, the representation is not as good, but still a reasonble approximation when precise accuracy is not paramount.

2.2 Shock Geometry

The conical shock wave attached to the elliptic cone is assumed to have the form (for $\alpha = 0$)

$$\theta_s = \beta - \varepsilon g \cos 2\phi + O(\varepsilon^2)\,, \qquad (2.9)$$

which is analogous to equation (2.7) for the body shape. Here β is the semivertex angle of the basic circular shock corresponding to the basic body with semivertex angle δ. The factor g is to be determined from the perturbation analysis. It, in effect, represents the deviation of the shock eccentricity from the body eccentricity.

By means of vector analysis, we find the unit outward normal on the shock to be given by

$$\hat{n}_s = \hat{e}_\theta - \frac{2\varepsilon g \sin 2\phi}{\sin\beta}\,\hat{e}_\phi + O(\varepsilon^2) \qquad (2.10)$$

This result is needed to establish the shock jump conditions.

a = 0.2555
b = 0.3562
e = 0.320

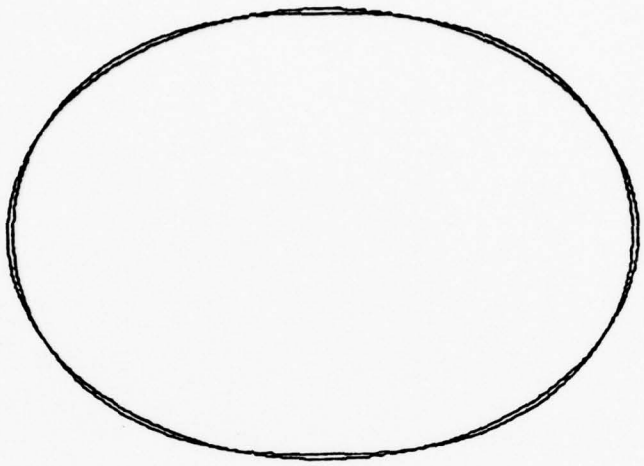

a = 0.2256
b = 0.4034
e = 0.523

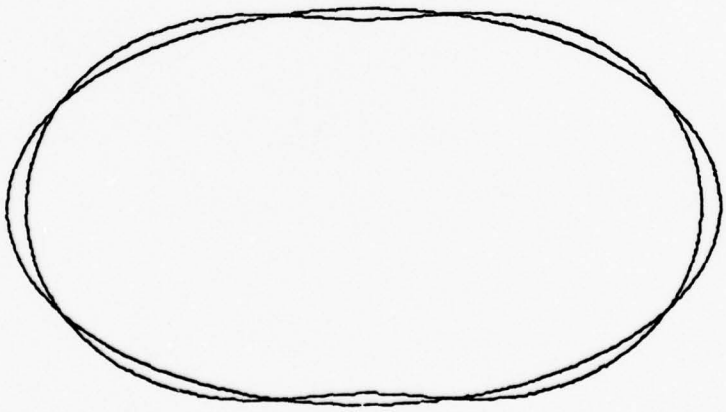

Figure 2.2 Two-Term Fourier Representation of the Ellipse

3. BOUNDARY CONDITIONS

3.1 Expansions for the Flow Variables

Let the velocity vector for conical flow be represented in spherical coordinates by

$$\vec{V} = u(\theta,\phi)\hat{e}_r + v(\theta,\phi)\hat{e}_\theta + w(\theta,\phi)\hat{e}_\phi \ . \qquad (3.1)$$

The Fourier representation for the body and shock shapes suggest that the velocity components, pressure, and density can be expanded in the following forms, valid outside the vortical layer adjacent to the body surface (for $\alpha = 0$):

$$u(\theta,\phi) = u_0(\theta) + \varepsilon u_1(\theta) \cos 2\phi + O(\varepsilon^2) \qquad (3.2a)$$

$$v(\theta,\phi) = v_0(\theta) + \varepsilon v_1(\theta) \cos 2\phi + O(\varepsilon^2) \qquad (3.2b)$$

$$w(\theta,\phi) = \varepsilon w_1(\theta) \sin 2\phi + O(\varepsilon^2) \qquad (3.2c)$$

$$p(\theta,\phi) = p_0(\theta) + \varepsilon p_1(\theta) \cos 2\phi + O(\varepsilon^2) \qquad (3.2d)$$

$$\rho(\theta,\phi) = \rho_0(\theta) + \varepsilon \rho_1(\theta) \cos 2\phi + O(\varepsilon^2) \qquad (3.2e)$$

The lowest-order terms, with the subscript naught, pertain to the basic circular-cone solution, which is presumed known.

3.2 Free Stream Normal Velocity at the Shock

The free stream velocity in spherical coordinates is given by

$$\vec{V}_\infty = V_\infty \left[\cos\theta \, \hat{e}_r - \sin\theta \, \hat{e}_\theta \right] \qquad (3.3)$$

At the shock, $\theta = \theta_s \equiv \beta - \varepsilon g \cos 2\phi$, we have to first order from

$\cos(\varepsilon g \cos 2\phi) \tilde{\approx} 1$, $\sin(\varepsilon g \cos 2\phi) \tilde{\approx} \varepsilon g \cos 2\phi$

$$\vec{V}_\infty = V_\infty \Big[\{\cos\beta + \varepsilon g \sin\beta \cos 2\phi\} \hat{e}_r - \{\sin\beta - \varepsilon g \cos\beta \cos 2\phi\} \hat{e}_\theta + O(\varepsilon^2) \Big] \qquad (3.4)$$

Using equation (2.10), we find the normal velocity at the shock to be, to first order,

$$\vec{V}_\infty \cdot \hat{n}_s = - V_\infty \sin \beta + \varepsilon g V_\infty \cos \beta \cos 2\phi + O(\varepsilon^2) \qquad (3.5)$$

3.3 Downstream Pressure at the Shock

The shock jump conditions give for the pressure ratio across the shock the well-known relation

$$\frac{p_s}{p_\infty} = 1 + \frac{2\gamma}{\gamma+1} \left(M_n^2 - 1\right) \qquad (3.6)$$

for a thermally and calorically perfect gas. Here γ is the ratio of specific heats, $\gamma \equiv c_p/c_v$, and $M_n \equiv \vec{V}_\infty \cdot \hat{n}/a_\infty$ is the normal free stream Mach number, a_∞ being the free stream speed of sound. Substituting (3.5) into (3.6) yields

$$\frac{p_s}{p_\infty} = 1 + \frac{2\gamma}{\gamma+1} \left(K_\beta^2 - 1\right) - \varepsilon \frac{4\gamma}{\gamma+1} K_\beta^2 g \cot \beta \cos 2\phi + O(\varepsilon^2) \qquad (3.7)$$

where $K_\beta \equiv M_\infty \sin \beta$.

Equation (3.2d) for the pressure evaluated at the shock reads

$$p(\theta_s, \phi) = p_0(\theta_s) + \varepsilon p_1(\theta_s) \cos 2\phi + O(\varepsilon^2) \qquad (3.8)$$

Transferring this value to the basic unperturbed shock by means of a Taylor expansion yields, to first order,

$$p(\theta_s, \phi) = p_0(\beta) + \varepsilon \left[- \left(\frac{dp_0}{d\theta}\right)_\beta g + p_1(\beta) \right] \cos 2\phi + O(\varepsilon^2) \qquad (3.9)$$

Identifying the first-order perturbation terms in (3.7) and (3.9) leads to the shock boundary conditions for the perturbation pressure

$$\frac{p_1(\beta)}{p_\infty} = - \frac{4\gamma}{\gamma+1} g K_\beta^2 \cot \beta + \frac{g}{p_\infty} \left(\frac{dp_0}{d\theta}\right)_\beta \qquad (3.10)$$

For the undisturbed conical flow, the pressure gradient can be evaluated in terms of the velocity gradient. Hence we have

$$\left(\frac{dp_o}{d\theta}\right)_\beta = \rho_\infty V_\infty \sin\beta \left[V_\infty \cos\beta + \left(\frac{dv_o}{d\theta}\right)_\beta \right] \qquad (3.11)$$

Thus, alternatively, the pressure boundary condition can be written

$$p_1(\beta) = \rho_\infty g\, V_\infty^2 \sin\beta \cos\beta \left[\frac{\gamma-3}{\gamma+1} + \left\{ \left(\frac{dv_o}{d\theta}\right)_\beta \Big/ V_\infty \cos\beta \right\} \right] \qquad (3.12)$$

The derivative $(dv_o/d\theta)_\beta$ can be evaluated in terms of the density ratio across the shock, as shown in the next section.

3.4 Downstream Density at the Shock

The pressure ratio across the shock is given by

$$\frac{\rho_\infty}{\rho_s} = \frac{(\gamma-1)\, M_n^2 + 2}{(\gamma+1)\, M_n^2} \quad . \qquad (3.13)$$

Expanding this expression analogously to that for the pressure, we obtain the shock density to first order:

$$\frac{\rho_\infty}{\rho_s} = \xi_o + \epsilon \xi_1 \cos 2\phi + O(\epsilon^2) \quad , \qquad (3.14a)$$

where

$$\xi_o \equiv \frac{\rho_\infty}{\rho_o(\beta)} = \frac{(\gamma-1)K_\beta^2 + 2}{(\gamma+1)\, K_\beta^2} \qquad (3.14b)$$

$$\xi_1 \equiv 2g \cot\beta \left[\xi_o - \frac{\gamma-1}{\gamma+1} \right] \qquad (3.14c)$$

An explicit expression for $\rho_1(\beta)$ is not needed. It can be shown from the basic cone solution that

$$\left(\frac{dv_o}{d\theta}\right)_\beta = - V_\infty \cos\beta \left[2 - \frac{\gamma-1}{\gamma+1}\, \xi_o \right] \qquad (3.15)$$

3.5 Downstream Velocity at the Shock

The velocity components immediately downstream of the shock are obtained from the governing conditions on the normal and tangential components. The normal components of the velocity is governed by the mass conservation equation:

$$(\vec{V}\cdot\hat{n})_s = \frac{\rho_\infty}{\rho_s}\ (\vec{V}_\infty\cdot\hat{n}_s) \tag{3.16}$$

The right side is determined to first order by means of (3.5) and (3.14):

$$(\vec{V}\cdot\hat{n})_s = -\xi_0 V_\infty \sin\beta + \varepsilon V_\infty(\xi_0 g\cos\beta - \xi_1\sin\beta)\cos 2\phi + O(\varepsilon^2) \tag{3.17}$$

The left side of the previous two equations is determined to first order from (2.10), (3.1), and (3.2) as

$$(\vec{V}\cdot\hat{n})_s = v_0(\theta_s) + \varepsilon v_1(\theta_s)\cos 2\phi + O(\varepsilon^2) \tag{3.18}$$

Transferring this value to the unperturbed shock yields

$$(\vec{V}\cdot\hat{n})_s = v_0(\beta) + \varepsilon\left[v_1(\beta) - g\left(\frac{dv_0}{d\theta}\right)_\beta\right]\cos 2\phi + O(\varepsilon^2) \tag{3.19}$$

Comparing equation (3.17) and (3.19) leads to the following results:

$$v_0(\beta) = -\xi_0 V_\infty \sin\beta \tag{3.20}$$

$$v_1(\beta) = -\xi_1 V_\infty \sin\beta + g\left[\xi_0 V_\infty\cos\beta + \left(\frac{dv_0}{d\theta}\right)_\beta\right] \tag{3.21a}$$

Utilizing (3.14c) for ξ_1 now gives

$$v_1(\beta) = g\left[\left\{\frac{2(\gamma-1)}{\gamma+1} - \xi_0\right\} V_\infty\cos\beta + \left(\frac{dv_0}{d\theta}\right)_\beta\right] \tag{3.21b}$$

The other two velocity components at the shock are determined from conservation of the tangential components:

$$\vec{V}_\infty \times \hat{n}_s = \vec{V}_s \times \hat{n}_s \tag{3.22}$$

Substitution of the first-order expansions and transfer of the conditions to the basic unperturbed shock yields

$$u_0(\beta) = V_\infty\cos\beta \tag{3.23}$$

$$u_1(\beta) = g\, V_\infty \sin\beta(1-\xi_0) \tag{3.24}$$

$$w_1(\beta) = -2gV_\infty(1-\xi_0) \tag{3.25}$$

The needed boundary conditions at the shock have now been specified.

3.6 Surface Boundary Condition

At the body surface, $\theta = \theta_c \equiv \delta - \varepsilon\cos 2\phi$, the normal velocity must vanish:

$$(\vec{V}\cdot\hat{n})_c = 0 \tag{3.26}$$

By means of vector analysis, we find the unit outward normal vector on the elliptic cone surface to be, to first order,

$$\hat{n}_c = \hat{e}_\theta - \frac{2\varepsilon \sin 2\phi}{\sin\delta}\,\hat{e}_\phi + O(\varepsilon^2) \tag{3.27}$$

Substituting this expression and the velocity expansions into (3.25) and transferring the boundary conditions to the basic circular cone surface leads to the surface boundary conditions

$$v_0(\delta) = 0 \tag{3.28}$$

$$v_1(\delta) = \left(\frac{dv_0}{d\theta}\right)_\delta \tag{3.29}$$

Equation (3.28), of course, is the tangency condition for the basic cone problem, and equation (3.29) is the surface boundary condition for the first-order perturbation. Rigorously, we should have obtained (3.29) by matching the outer expansion with an inner expansion for the vortical layer adjacent to the cone surface. Such an analysis shows that equation (3.29) is indeed proper [14,15].

4. PERTURBATION EQUATIONS

The pressure, density, and velocity are governed by the equations of change for mass, momentum, and energy, plus appropriate equations of state. Here we assume the flow is inviscid, nonconducting, steady, and behaves as a thermally and calorically perfect gas. We wish first to obtain expressions for the pressure and density perturbations in terms of the velocities, and then finally to obtain a single equation for only one of the perturbation velocity components.

4.1 Energy Equation

For steady flow, the energy equation can be expressed in terms of the entropy, s, as

$$\vec{V}\cdot\text{grad } s = 0 \tag{4.1}$$

Thus the flow on either side of the shock is isentropic, that is, the entropy along a streamline is a constant. Of course, the uniform flow upstream of the shock is homentropic since the entropy is the same on every streamline before it passes through the shock. If the entropy is expanded in the form

$$s(\theta,\phi) = s_0(\theta) + \varepsilon s_1(\theta) \cos 2\phi + O(\varepsilon^2) \tag{4.2}$$

then expansion of equation (4.1) leads to the result that s_0 is a constant and that s_1 is also a constant. Thus the zeroth-order flow past the basic cone is homentropic downstream of the shock. Since s_1 is a constant, the first-order entropy perturbation depends only on the azimuthal angle ϕ. This result is not valid on the body surface because the body surface is a stream surface that has a constant entropy, since grad s is a vector that is perpendicular to the surface $s(\theta,\phi)$ = constant and is also perpendicular to the velocity $\vec{V}$ which is tangent to the body surface. Thus expansion

(4.2) is not valid in a thin layer, called the vortical layer, adjacent to the body surface. Only the pressure and azimuthal velocity are uniformly valid across the vortical layer.

From the thermodynamic state relation for a perfect gas

$$\frac{ds}{c_v} = \frac{dp}{p} - \gamma \frac{d\rho}{\rho} \quad , \tag{4.3}$$

we can deduce that the first-order pressure and density perturbation satisfy the relation

$$\frac{p_1(\theta)}{p_0(\theta)} - \gamma \frac{\rho_1(\theta)}{\rho_0(\theta)} = \frac{s_1}{c_v} = \text{constant} \tag{4.4}$$

Another relation between the pressure and density perturbation can be found from energy considerations. Since the uniform flow upstream of the shock is homenergic (constant total enthalpy) and homenergic across the shock, it is also homenergic downstream of the shock. Thus we have for a perfect gas

$$\frac{\gamma}{\gamma-1} \frac{p}{\rho} + \frac{V^2}{2} = \frac{\gamma}{\gamma-1} \frac{p_\infty}{\rho_\infty} + \frac{V_\infty^2}{2} = \text{constant} \tag{4.5}$$

Substituting the perturbation forms (3.2) into this equation and extracting the first-order perturbation yields

$$\frac{p_1(\theta)}{p_0(\theta)} - \frac{\rho_1(\theta)}{\rho_0(\theta)} = - \frac{\gamma-1}{\gamma} \frac{\rho_0}{p_0} (u_0 u_1 + v_0 v_1) \tag{4.6}$$

This is a relation between the pressure and density perturbations in terms of the velocity perturbation.

Equations (4.4) and (4.6) can be solved separately for the pressure and density perturbations. We obtain

$$\rho_1(\theta) = \frac{- \rho_0 (u_0 u_1 + v_0 v_1)}{a_0^2} + \rho_0 F_1 \tag{4.7}$$

$$p_1(\theta) = - \rho_0(u_0 u_1 + v_0 v_1) + p_0 F_1 \qquad (4.8)$$

where $a_0^2(\theta) \equiv \gamma p_0/\rho_0$ is the speed of sound squared in the basic unperturbed flow, and

$$F_1 \equiv - \frac{s_1}{(\gamma-1)\, c_v} = \text{constant} \qquad (4.9)$$

The pressure and density perturbations are thus determined in terms of the velocity perturbations. The constant F_1 can be obtained from the shock boundary conditions. Thus we obtain

$$F_1 = \frac{p_1(\beta)}{p_0(\beta)} + \frac{\rho_0(\beta)}{p_0(\beta)} \left[u_0(\beta)\, u_1(\beta) + v_0(\beta)\, v_1(\beta) \right]$$

$$= \gamma g\, V_\infty^2 \sin\beta \cos\beta\, (1-\xi_0)^2/a_0^2(\beta) \qquad (4.10)$$

4.2 Momentum Equation

The momentum equation for inviscid steady flow is

$$\rho \left[\nabla \left(\frac{V^2}{2} \right) - \vec{V} \times \vec{\Omega} \right] = - \nabla p \,, \qquad (4.11)$$

where $\vec{\Omega} = \text{curl}\ \vec{V}$ *is the vorticity vector. For the vector quantities let*

$$\vec{V} = \vec{V}_0 + \varepsilon \vec{v}_1 + O(\varepsilon^2) \qquad (4.12a)$$

$$\vec{\Omega} = \varepsilon \vec{\Omega}_1 + O(\varepsilon^2) \qquad (4.12b)$$

where $\vec{\Omega}_1 = \text{curl}\ \vec{v}_1$ and the spherical components of the first-order perturbation velocity $\vec{v}_1$ can be ascertained from equations (3.2). When the perturbation expansions are *substituted into equation* (4.11), *the first-order* perturbation equation can be extracted, and it is

$$(\rho_1 \cos 2\phi)\ \nabla\left(\frac{V_o^2}{2}\right) + \rho_o \nabla(\vec{V}_o \cdot \vec{v}_1) - \rho_o \vec{V}_o \times \vec{\Omega}_1 = -\nabla(p_1 \cos 2\phi) \tag{4.13}$$

The first-order vorticity perturbation has the components

$$\Omega_{1_r} = \frac{\sin 2\phi}{r \sin\theta}\left[\frac{d}{d\theta}(w_1 \sin\theta) + 2v_1\right] \tag{4.14a}$$

$$\Omega_{1_\theta} = -\frac{\sin 2\phi}{r \sin\theta}\left[2u_1 + w \sin\theta\right] \tag{4.14b}$$

$$\Omega_{1_\phi} = \frac{\cos 2\phi}{r}\left[v_1 - \frac{du_1}{d\theta}\right] \tag{4.14c}$$

We also have

$$\vec{V}_o \times \vec{\Omega}_1 = \hat{e}_r(v_o \Omega_{1_\phi}) - \hat{e}_\theta(u_o \Omega_{1_\phi}) + \hat{e}_\phi(u_o \Omega_{1_\theta} - v_o \Omega_{1_r}) \tag{4.15}$$

From equation (4.13) it can be determined that

$$(\vec{V}_o \times \vec{\Omega}_1) \cdot \hat{e}_r = 0 \tag{4.16}$$

It follows from (4.15) that $\Omega_{1_\phi} = 0$, and hence that

$$v_1 = \frac{du_1}{d\theta} \tag{4.17}$$

Thus equation (4.15) reduces to

$$\vec{V}_o \times \vec{\Omega}_1 = \hat{e}_\phi(u_o \Omega_{1_\theta} - v_o \Omega_{1_r}) \tag{4.18}$$

The ϕ-component of equation (4.13) can be written as

$$u_o \Omega_{1_\theta} - v_o \Omega_{1_r} = -2\left[\frac{p_1}{\rho_o} + u_o u_1 + v_o v_1\right]\frac{\sin 2\phi}{r \sin\theta} \tag{4.19}$$

The pressure perturbation p_1 can be eliminated by means of equation (4.8), and we get

$$u_o \Omega_{1_\theta} - v_o \Omega_{1_r} = \frac{-2a_o^2 F_1}{\gamma}\ \frac{\sin 2\phi}{r \sin\theta} \tag{4.20}$$

where $a_o^2(\theta) \equiv \gamma p_o/\rho_o$ and F_1 is a constant given by (4.10). By means of (4.14a,b) we can further rewrite (4.20) as

$$v_o \frac{d}{d\theta}\left[2u_1 + w_1 \sin\theta\right] + u_o\left[2u_1 + w_1 \sin\theta\right] = \frac{2F_1}{\gamma} a_o^2(\theta) \tag{4.21}$$

Introducing the integration factor

$$I(\theta) \equiv \exp\left[\int_\beta^\theta \left(\frac{u_o}{v_o}\right) d\theta\right], \tag{4.22}$$

we can integrate equation (4.21) and obtain

$$2u_1 + w_1 \sin\theta = \frac{2F_1}{\gamma}\ \frac{1}{I}\int_\beta^\theta \frac{a_o^2\, I}{v_o}\ d\theta \tag{4.23}$$

The constant of integration vanishes by virtue of the shock boundary conditions (3.24) and (3.25).

Equations (4.17) and (4.23) give v_1 and w_1 in terms of u_1. It remains to find a single equation for u_1.

4.3 Continuity Equation

Mass conservation is described by the continuity equation

$$\mathrm{div}(\rho\vec{V}) = 0 \tag{4.24}$$

When the perturbation expansions are substituted into this equation and the first-order perturbation extracted, we get

$$\mathrm{div}\ (\rho_1 \cos 2\phi\ \vec{V}_o + \rho_o \vec{v}_1) = 0 \tag{4.25}$$

With the basic-flow result $\mathrm{div}(\rho_o \vec{V}_o) = 0$ accounted for, this equation can be rearranged to read

$$\mathrm{div}\ \vec{v}_1 = -\vec{V}_o \cdot \nabla\left(\frac{\rho_1 \cos 2\phi}{\rho_o}\right) - \frac{\vec{v}_1}{\rho_o} \cdot \nabla\rho_o \tag{4.26}$$

If it were assumed that the density varies so slowly that it is approximately a constant, then the right side of equation (4.26) can be set equal to zero as an approximation, and a relatively simple equation for $\vec{v}_1$ ensues. (The right side does vanish at the body surface, $\theta = \delta$.) This so-called constant-density approximation leads to remarkably accurate results for the basic-flow solution and for the flow past a circular cone at angle of attack [12,13]. These constant-density approximations were justified a posteriori by comparison with extensive numerical tabulated results. Such comparisons are not so available for the elliptic-cone problem of present interest, and hence we must devote more attention to the terms on the right side of equation (4.26).

In equation (4.26), let us now eliminate $\rho_1(\theta)$ by equation (4.7) and utilize the following basic-flow results:

$$\frac{a_o^2}{\rho_o}\frac{d\rho_o}{d\theta} = \frac{1}{\rho_o}\frac{dp_o}{d\theta} = \frac{1}{\gamma-1}\frac{da_o^2}{d\theta} = -\frac{d}{d\theta}\left(\frac{\vec{V}_o^2}{2}\right) \tag{4.27}$$

Equation (4.26) can now be expanded and written in the form

$$\left[1 - A\right]\frac{dv_1}{d\theta} + \cot\theta\left[1 - B\right]v_1 + \left(2 - \frac{4}{\sin^2\theta} - C\right)u_1 = -\frac{2(2u_1+w_1\sin\theta)}{\sin^2\theta}$$

where (4.28)

$$A(\theta) \equiv \frac{v_o^2}{a_o^2} \tag{4.29a}$$

$$B(\theta) \equiv \tan\theta\,\frac{v_o}{a_o^2}\left(u_o + \frac{dv_o}{d\theta}\right)\left\{2 + (\gamma-1)\frac{v_o^2}{a_o^2}\right\} \tag{4.29b}$$

$$C(\theta) \equiv \frac{v_o^2}{a_o^2}\left\{1 + (\gamma-1)\frac{u_o}{a_o^2}\left(u_o + \frac{dv_o}{d\theta}\right)\right\} \tag{4.29c}$$

The factors A, B, and C in equation (4.28) are variable coefficients, and they stem from the right side of equation (4.26). At the cone surface $\theta = \delta_o$, the factors A, B, and C all vanish since $v_o(\delta) = 0$. At the shock surface $\theta = \beta$, the factors A, B, and C take the values

$$A(\beta) = \frac{2\xi_o}{(\gamma+1) - \xi_o(\gamma-1)} \quad , \tag{4.30a}$$

$$B(\beta) = \frac{4}{(\gamma+1) - \xi_o(\gamma-1)} \quad , \tag{4.30b}$$

$$C(\beta) = \frac{\xi_o - 2\,\frac{\gamma-1}{\gamma+1}\,\cot^2\beta}{(\gamma+1) - \xi_o(\gamma-1)} \quad , \tag{4.30c}$$

where the undisturbed shock density ratio, ξ_o, is given by (3.14b). In the hypersonic limit, $K_\beta = \infty$ and $A(\beta)$ takes the value $(\gamma-1)/2\gamma$. Thus for $\gamma = 7/5$, $A(\beta) = 1/7$ for $K_\beta = \infty$. For hypersonic flow it is thus safe to neglect $A(\theta)$ compared to unity. Since $A(\theta_o) = 0$, it is thus reasonable to neglect $A(\theta)$ always except perhaps very near sonic conditions, for which $A(\beta) = 1$ when $K_\beta = 1$. Likewise $C(\beta)$ is small compared to $(2 - 4\,\csc^2\beta)$ in the coefficient of u_1 for all values of K_β. Thus $C(\theta)$ should be negligible in general since it also vanishes at $\theta = \delta$. The factor $B(\beta)$ varies between $(\gamma+1)/\gamma$ for $K_\beta = \infty$ and 2 for $K_\beta = 1$, and thus apparently should not be neglected compared to unity. Moreover, the factor (1-B) changes sign between the shock and the body. On the other hand, if A, B, and C are all neglected, the resulting differential equation still behaves properly at the body surface since A, B, and C vanish there anyway. In addition, the resulting second-order differential equation must satisfy the two boundary conditions for $u_1(\beta)$ and $v_1(\beta)$ at the shock.

Thus, even though A, B, and C be neglected, the resulting solution should behave properly at both sides of the shock layer, and presumably also in between. As mentioned earlier, neglecting A, B, and C yields good results for the circular cone at angle of attack.

Even though we intend eventually to obtain an approximate solution by neglecting A, B, and C, we can justify the results still further by recasting the differential equation as an integral equation. Replacing v_1 by (4.17) and w_1 by (4.23), we can rewrite equation (4.28) as

$$u_1'' + \cot\theta\, u_1' + (2 - 4\csc^2\theta)u_1 = -\frac{4F_1}{\gamma}\frac{H_o(\theta)}{\sin^2\theta} + H_1(\theta) \quad (4.31)$$

where

$$H_o(\theta) \equiv \frac{1}{I}\int_\beta^\theta \frac{a_o^2 I}{v_o}\, d\theta \quad (4.32a)$$

$$H_1(\theta) \equiv Au_1'' + B\cot\theta\, u_1' + Cu_1 \quad (4.32b)$$

When H_o and H_1 vanish, a solution to equation (4.31) is $u_1 = \csc^2\theta$. This suggests the substitution

$$u_1 = \frac{X(\theta)}{\sin^2\theta} \quad (4.33)$$

Equation (4.31) can now be written

$$\left(\frac{X'}{\sin^3\theta}\right)' = -\frac{4F_1}{\gamma}\frac{H_o(\theta)}{\sin^3\theta} + \frac{H_1(\theta)}{\sin\theta} \quad (4.34)$$

Two integrations yield

$$X(\theta) = X(\beta) + \frac{X'(\beta)}{\sin^3\beta}\int_\beta^\theta \sin^3\theta\, d\theta \quad (4.35)$$

$$-\frac{4F_1}{\gamma}\int_\beta^\theta\left[\sin^3\theta\int_\beta^\theta\frac{H_o(\theta)}{\sin^3\theta}\, d\theta\right] d\theta + \int_\beta^\theta\left[\sin^3\theta\int_\beta^\theta\frac{H_1(\theta)d\theta}{\sin\theta}\right] d\theta$$

where

$$X(\beta) = u_1(\beta) \sin^2 \beta$$

$$= g V_\infty \sin^3\beta (1 - \varepsilon_o) \tag{4.36a}$$

$$X'(\beta) = g \sin^2\beta \left[\left(\frac{4\gamma}{\gamma+1} - 3\xi_o\right) V_\infty \cos \beta + \left(\frac{dv_o}{d\theta}\right)_\beta\right] \tag{4.36b}$$

When $X(\theta)$ is known, the velocity components are determined by

$$u_1(\theta) = X(\theta)/\sin^2 \theta \tag{4.37a}$$

$$v_1(\theta) = \left[X'(\theta) - 2X(\theta) \cot\theta\right]/\sin^2 \theta \tag{4.37b}$$

$$w_1(\theta) = \left[- 2u_1(\theta) + \frac{2F_1}{\gamma} H_o(\theta)\right] / \sin \theta \tag{4.37c}$$

The shock eccentricity factor g is determined by satisfying the surface boundary condition (3.29) and then solving for g. Equation (4.35) is an integral equation because the unknown function $X(\theta)$ also appears in the function $H_1(\theta)$.

5. APPROXIMATE SOLUTION FOR HYPERSONIC FLOW

5.1 Basic Cone Flow Approximations

For hypersonic flow in the limit $M_\infty \to \infty$ and $\sin\theta \to 0$ such that the combination $K \equiv M_\infty \sin\theta$ remains finite, the basic cone flow can be approximated accurately by [10,11]

$$\frac{u_o(\theta)}{V_\infty} = 1 - \frac{\sin^2\delta}{2}\left[\frac{\sin^2\theta}{\sin^2\delta} + \ln\left(\frac{\sin^2\beta}{\sin^2\theta}\right)\right] \tag{5.1a}$$

$$\frac{v_o(\theta)}{V_\infty} = -\sin\theta\left[1 - \frac{\sin^2\delta}{\sin^2\theta}\right] \tag{5.1b}$$

and the relation between the shock and body angles is given by

$$\frac{\sin\beta}{\sin\delta} = \sqrt{\frac{\gamma+1}{2} + \frac{1}{(M_\infty \sin\delta)^2}} \tag{5.1c}$$

Let us now restrict ourselves to small angles such that $\sin\theta \simeq \theta$ and neglect second-order terms in (5.1). Then we get

$$\frac{u_o}{V_\infty} \simeq 1 \tag{5.2a}$$

$$\frac{v_o}{V_\infty} \simeq -\theta\left(1 - \frac{\delta^2}{\theta^2}\right) \tag{5.2b}$$

$$\frac{\beta}{\delta} = \sqrt{\frac{\gamma+1}{2} + \frac{1}{K_\delta^2}} \tag{5.2c}$$

where $K_\delta \equiv M_\infty \delta$ is the hypersonic similarity parameter.

5.2 Evaluation of the Integrals

With the approximations (5.2a,b), the integrating factor I becomes

$$I = \left[\frac{\beta^2 - \delta^2}{\theta^2 - \delta^2} \right]^{1/2} \tag{5.3}$$

In the evaluation of the function $H_o(\theta)$ given by (4.32a), the speed of sound squared $a_o^2(\theta)$ varies only by a few percent across the shock layer. Hence we replace it by $a_o^2(\beta)$, and the function $H_o(\theta)$ becomes

$$H_o(\theta) = \frac{a_o^2(\beta)}{V_\infty} \left\{ 1 - \sqrt{\frac{\theta^2 - \delta^2}{\beta^2 - \delta^2}} \right\} \tag{5.4}$$

We then obtain

$$\int_\beta^\theta \frac{H_o(\theta)}{\theta^3} d\theta = \frac{a_o^2(\beta)}{2V_\infty} \left[\frac{1}{\theta^2} \left\{ \sqrt{\frac{\theta^2 - \delta^2}{\beta^2 - \delta^2}} - 1 \right\} + \frac{1}{\delta \sqrt{\beta^2 - \delta^2}} \left\{ \cos^{-1} \frac{\delta}{\beta} - \cos^{-1} \frac{\delta}{\theta} \right\} \right] \tag{5.5}$$

$$\int_\beta^\theta \left[\theta^3 \int_\beta^\theta \frac{H_o(\theta)}{\theta^3} d\theta \right] d\theta = \frac{a_o^2(\beta)}{4V_\infty} \left[\sqrt{\frac{\theta^2 - \delta^2}{\beta^2 - \delta^2}} \left(\frac{5}{6} \theta^2 - \frac{\delta^2}{3} \right) \right.$$

$$\left. + \frac{\theta^4}{2\delta \sqrt{\beta^2 - \delta^2}} \left\{ \cos^{-1} \frac{\delta}{\beta} - \cos^{-1} \frac{\delta}{\theta} \right\} + \frac{\beta^2}{6} + \frac{\delta^2}{3} - \theta^2 \right] \tag{5.6}$$

5.3 Approximation for the Velocity

The first approximation solution for the integral equation (4.35) is obtained by neglecting the integral involving $H_1(\theta)$, which is the same as omitting the factors A, B, and C in the original differential equation. We thus get

$$u_1(\theta) = \frac{X(\beta)}{\theta^2} + \frac{X'(\beta)}{4\beta^3 \theta^2} (\theta^4 - \beta^4) + \frac{f_1}{2} \left[\sqrt{\frac{\theta^2 - \delta^2}{\beta^2 - \delta^2}} \left(\frac{5}{6} - \frac{\delta^2}{3\theta^2} \right) \right.$$

$$\left. + \frac{\theta^2}{2\delta \sqrt{\beta^2 - \delta^2}} \left\{ \cos^{-1} \frac{\delta}{\beta} - \cos^{-1} \frac{\delta}{\theta} \right\} + \frac{\beta^2}{6\theta^2} + \frac{\delta^2}{3\theta^2} - 1 \right] \tag{5.7}$$

$$v_1(\theta) = -\frac{2X(\beta)}{\theta^3} + \frac{X'(\beta)}{2}\left(\frac{\theta}{\beta^3} + \frac{\beta}{\theta^3}\right) + f_1\left[\frac{1}{\theta}\sqrt{\frac{\theta^2-\delta^2}{\beta^2-\delta^2}}\left(\frac{1}{6}+\frac{\delta^2}{3\theta^2}\right)\right.$$

$$\left. + \frac{\theta}{2\delta\sqrt{\beta^2-\delta^2}}\left(\cos^{-1}\frac{\delta}{\beta} - \cos^{-1}\frac{\delta}{\theta}\right) - \frac{\beta^2}{6\theta^3} - \frac{\delta^2}{3\theta^3}\right] \qquad (5.8)$$

$$w_1(\theta) = -\frac{2X(\beta)}{\theta^3} - \frac{X'(\beta)}{2\beta^3\theta^3}(\theta^4 - \beta^4) - f_1\left[\frac{1}{\theta}\sqrt{\frac{\theta^2-\delta^2}{\beta^2-\delta^2}}\left(-\frac{1}{6}-\frac{\delta^2}{3\theta^2}\right)\right.$$

$$\left. + \frac{\theta}{2\delta\sqrt{\beta^2-\delta^2}}\left(\cos^{-1}\frac{\delta}{\beta} - \cos^{-1}\frac{\delta}{\theta}\right) + \frac{\beta^2}{6\theta^3} + \frac{\delta^2}{3\theta^3}\right] \qquad (5.9)$$

where

$$f_1 \equiv \frac{-2F_1 a_0^2(\beta)}{\gamma V_\infty} = -2gV_\infty \sin\beta\cos\beta(1-\xi_0)^2$$

$$\simeq -2gV_\infty\beta(1-\xi_0)^2 \qquad (5.10)$$

$$X(\beta) \simeq gV_\infty\beta^3(1-\xi_0) \qquad (5.11a)$$

$$X'(\beta) \simeq g\beta^2\left[\left(\frac{4\gamma}{\gamma+1} - 3\xi_0\right)V_\infty + \left(\frac{dv_0}{d\theta}\right)_\beta\right] \qquad (5.11b)$$

$$\simeq \frac{2}{\gamma+1}gV_\infty\beta^2\left[(\gamma-1) - \xi_0(\gamma+1)\right] \qquad (5.11c)$$

Expression (5.11c) is the approximation consistent with the velocity approximation (5.26b), that is,

$$\left(\frac{dv_0}{d\theta}\right)_\beta \simeq -V_\infty\left(1+\frac{\delta^2}{\beta^2}\right) \qquad (5.12a)$$

$$\simeq -V_\infty(2-\xi_0) \qquad (5.12b)$$

since

$$\xi_o \simeq 1 - \frac{\delta^2}{\beta^2} \tag{5.12c}$$

5.4 Shock Eccentricity Factor

The shock eccentricity factor, g, can now be determined from the condition

$$v_1(\delta) = \left(\frac{dv_o}{d\theta}\right)_\delta \simeq -2V_\infty \tag{5.13}$$

Solving for g from equation (5.8) yields

$$\frac{1}{g} = (1 - \xi_o)^2 \left\{ \frac{\beta \cos^{-1}\frac{\delta}{\beta}}{2\sqrt{\beta^2 - \delta^2}} - \frac{\beta^3}{6\delta^3} - \frac{\beta}{3\delta} \right\} + (1 - \xi_o)\frac{\beta^3}{\delta^3}$$

$$+ \frac{1}{2}\left\{\xi_o - \frac{\gamma-1}{\gamma+1}\right\}\left\{\frac{\delta}{\beta} + \frac{\beta^3}{\delta^3}\right\} \tag{5.14}$$

Denoting the basic-cone shock-body ratio by

$$\sigma \equiv \frac{\beta}{\delta} = \sqrt{\frac{\gamma+1}{2} + \frac{1}{K_\delta^2}} \quad , \tag{5.15}$$

we then get

$$\frac{1}{g} = \frac{1}{6\sigma^3}\left[\frac{3\cos^{-1}\left(\frac{1}{\sigma}\right)}{\sqrt{\sigma^2 - 1}} + \frac{6}{\gamma+1}(\sigma^6 + \sigma^2) + 3\sigma^4 - \sigma^2 - 5\right] \tag{5.16}$$

The shock eccentricity factor, g, is plotted in Fig. 5.1 as a function of K_δ for $\gamma = 7/5$. For $K_\delta \to 0$, which corresponds to the limit of linearized theory, the eccentricity factor tends to zero, $g \to 0$, that is, the shock tends to a circular Mach cone. For the limiting hypersonic flow, $K_\delta \to \infty$, g approaches the asymptote $g = 0.955$, and the shock tends to embrace the elliptic cone body. The shock, however, is always less eccentric than the body. When $K_\delta \to \infty$ and $\gamma \to 1$, then $\infty \to \delta$ and

$g \to 1$, and the shock embraces the body, in agreement with hypersonic Newtonian theory. The angle-of-attack shock eccentricity factor, $\tilde{g}$, obtained in Section 7, is also shown in Fig. 5.1 for comparison.

5.5 Shock-Layer Velocity Profiles

The first approximation for the velocity u_1, given by equation (5.7), is plotted in Fig. 5.2. The hypersonic similarity form gives $u_1/V_\infty\delta$ as a function of θ/δ, K_δ, and γ. Because the thickness of the shock layer varies as a function of K_δ, the shock layer is normalized by means of the variable

$$\tilde{\theta} = \frac{\theta - \delta}{\beta - \delta} \quad . \tag{5.17}$$

The body surface corresponds to $\tilde{\theta} = 0$ and the shock surface to $\tilde{\theta} = 1$. At the body surface $u_1/V_\infty\delta$ is insensitive to variations in K_δ, having approximately the value unity. At the shock surface, $u_1/V_\infty\delta$ is quite sensitive to variations in K_δ. In the hypersonic limit $K_\delta = \infty$, $u_1/V_\infty\delta$ increases only slightly from the shock to the body.

The velocity perturbation v_1/V_∞ is shown in Fig. 5.3 as a function of $\tilde{\theta}$, $\gamma = 1.4$, and various values of K_δ. The variation of v_1/V_∞ across the shock layer is analogous to the variation of $u_1/V_\infty\delta$, except that v_1/V_∞ is equal to -2, as imposed by the boundary condition (5.13).

The azimuthal velocity perturbation w_1/V_∞ is shown in Fig. 5.4 as a function of $\tilde{\theta}$, $\gamma = 1.4$, and various values of K_δ. At the shock surface, w_1/V_∞ increases as K_δ increases. For $K_\delta \simeq 2$, the variation of w_1/V_∞ across the shock layer is very slight. At the body surface, w_1/V_∞ decreases as K_δ increases. This is shown also in Fig. 5.5. When $K_\delta \to 0$, $w_1(\delta)/V_\infty \to -2$, which is in agreement with linearized theory. In

$$\theta_s = \beta + \alpha\tilde{g} \cos \phi - \varepsilon g \cos 2\phi$$

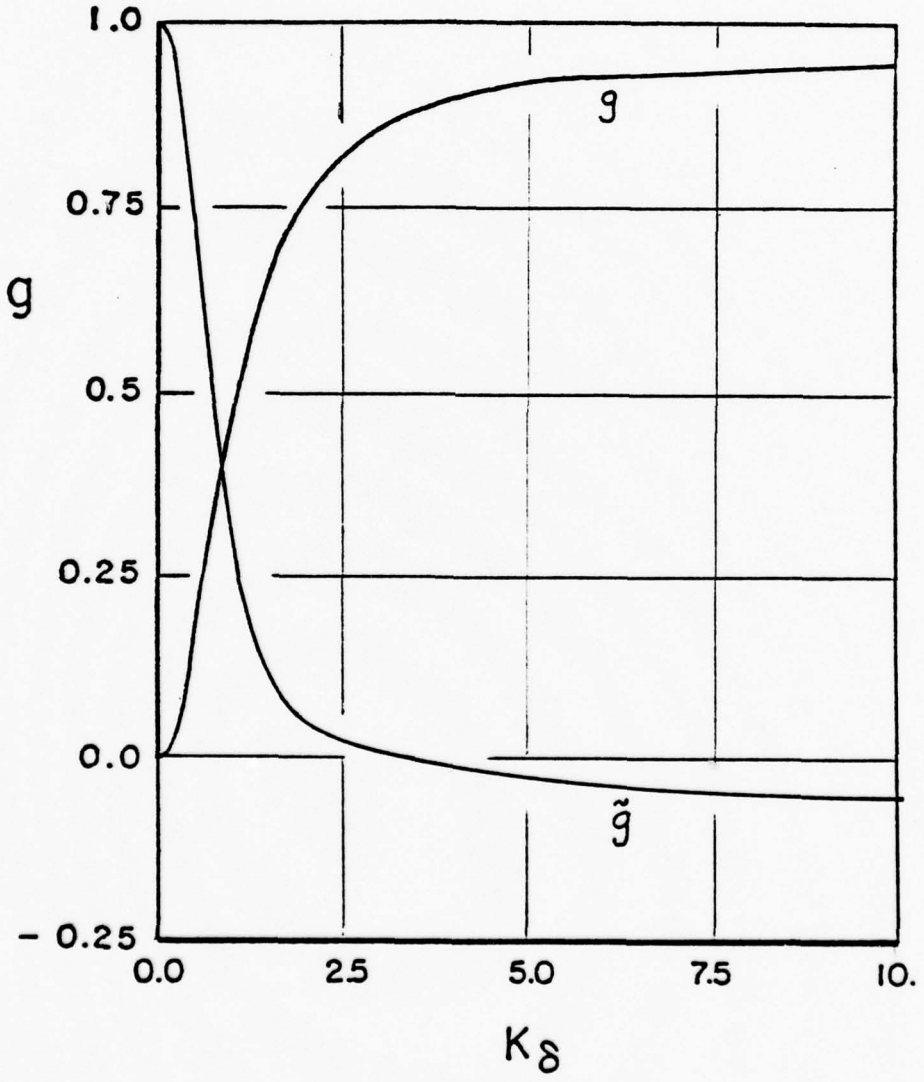

Figure 5.1 Shock Eccentricity Factors, $\gamma = 1.4$

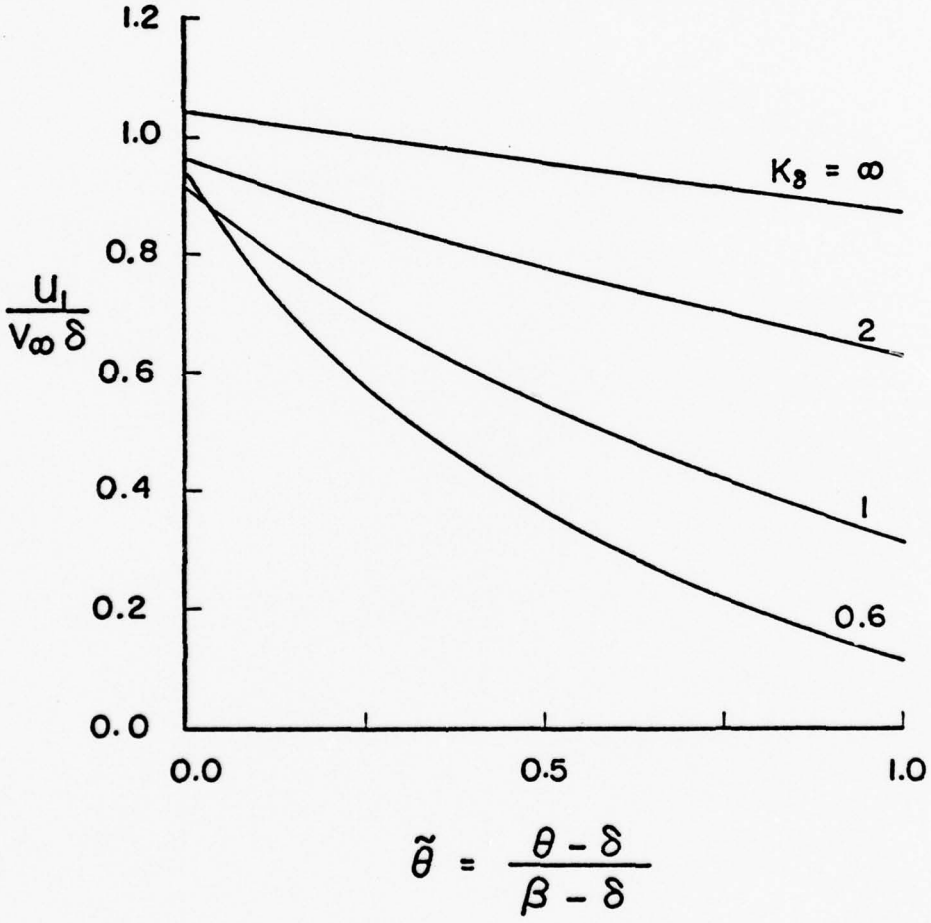

Figure 5.2. Radial Perturbation Velocity, $\gamma = 1.4$

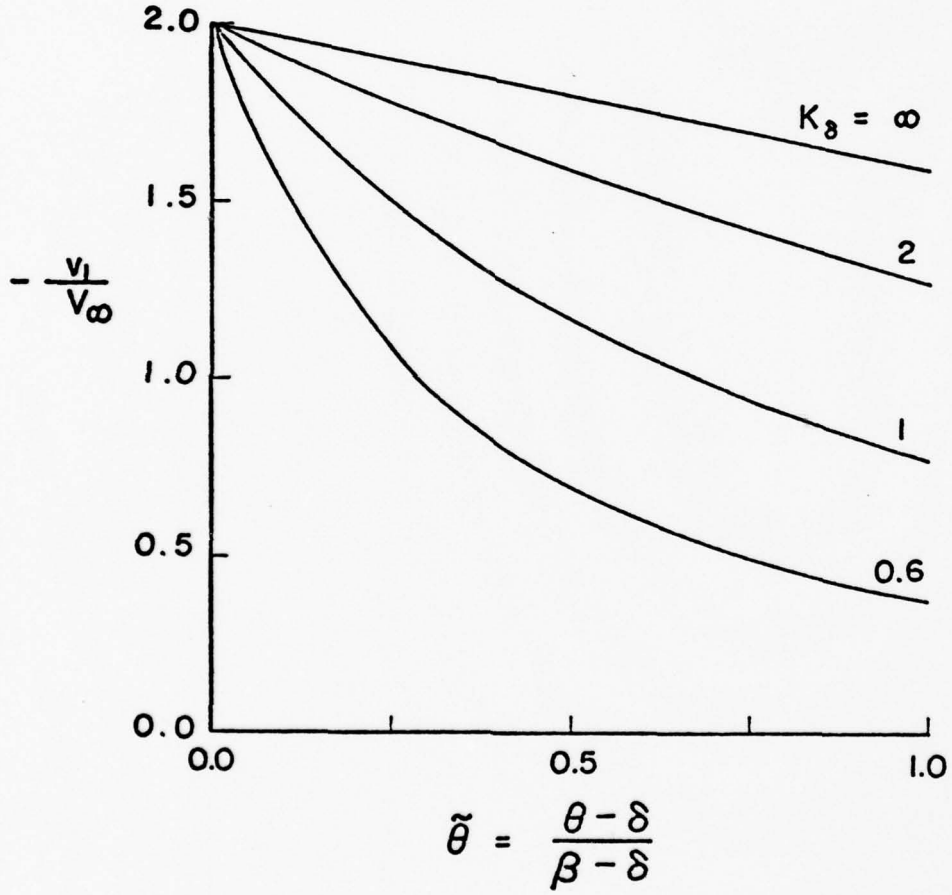

Figure 5.3. Polar Perturbation Velocity Components, $\gamma = 1.4$

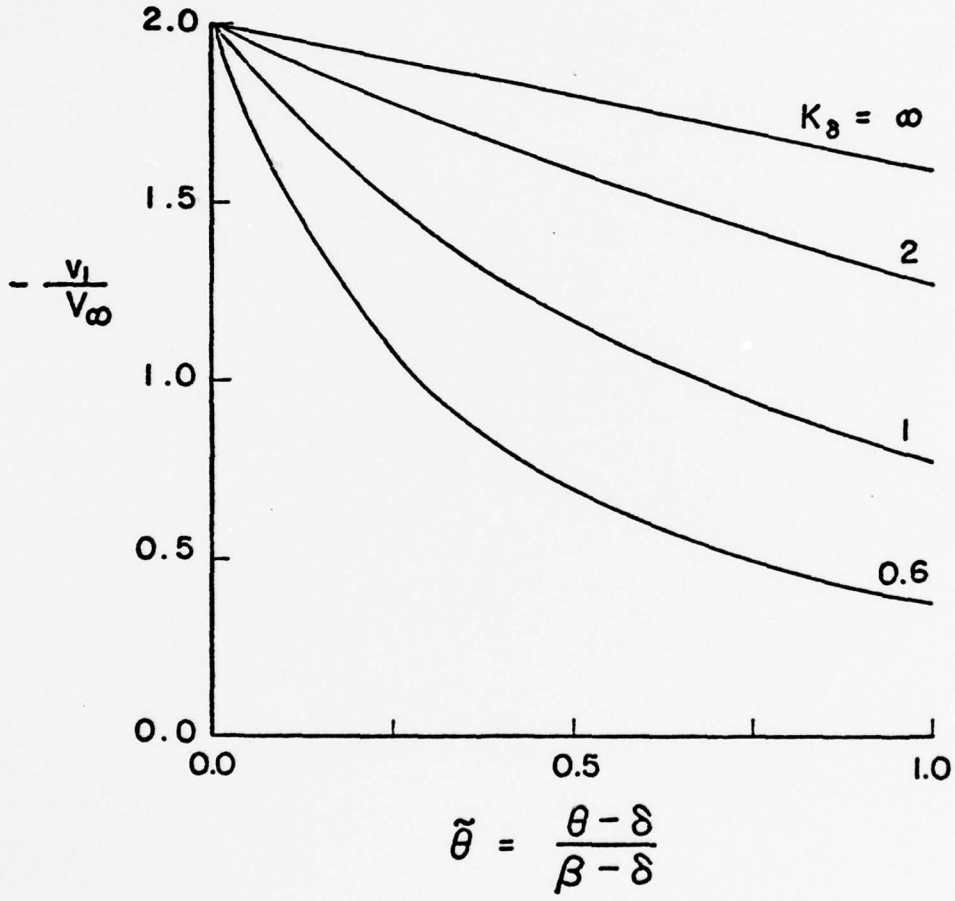

Figure 5.3. Polar Perturbation Velocity Components, $\gamma = 1.4$

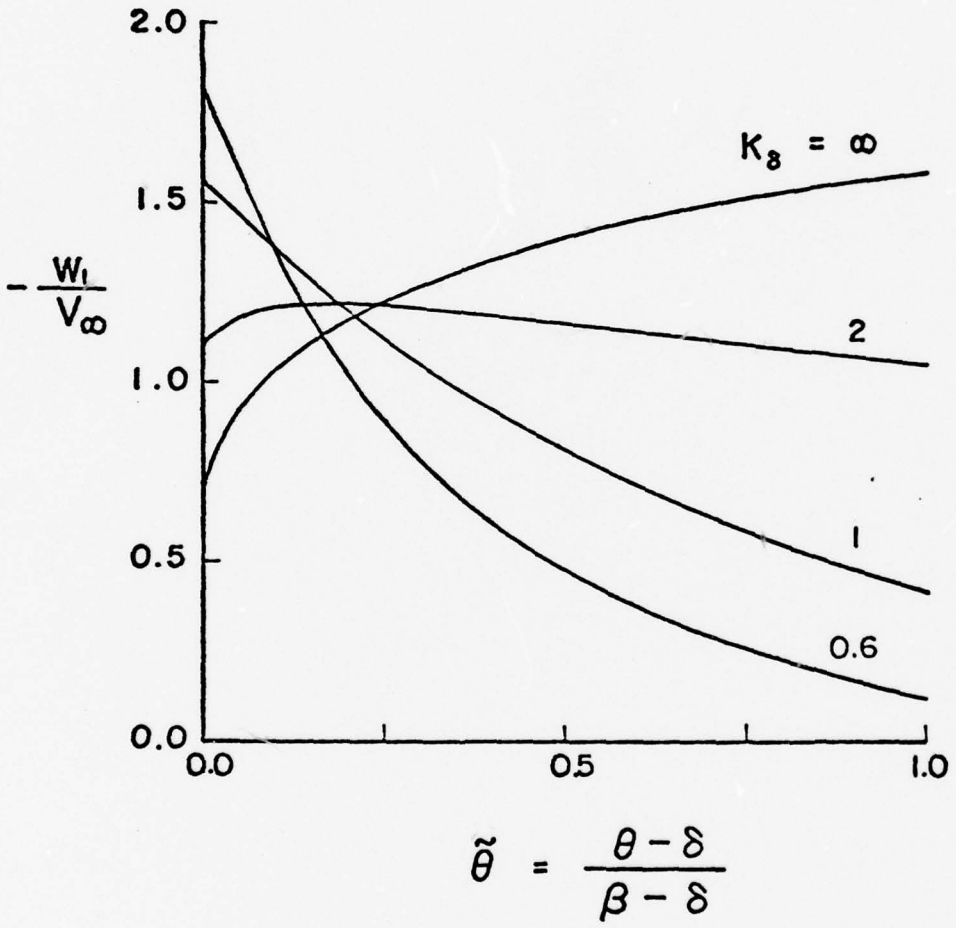

Figure 5.4. Azimuthal Perturbation Velocity Components, $\gamma = 1.4$

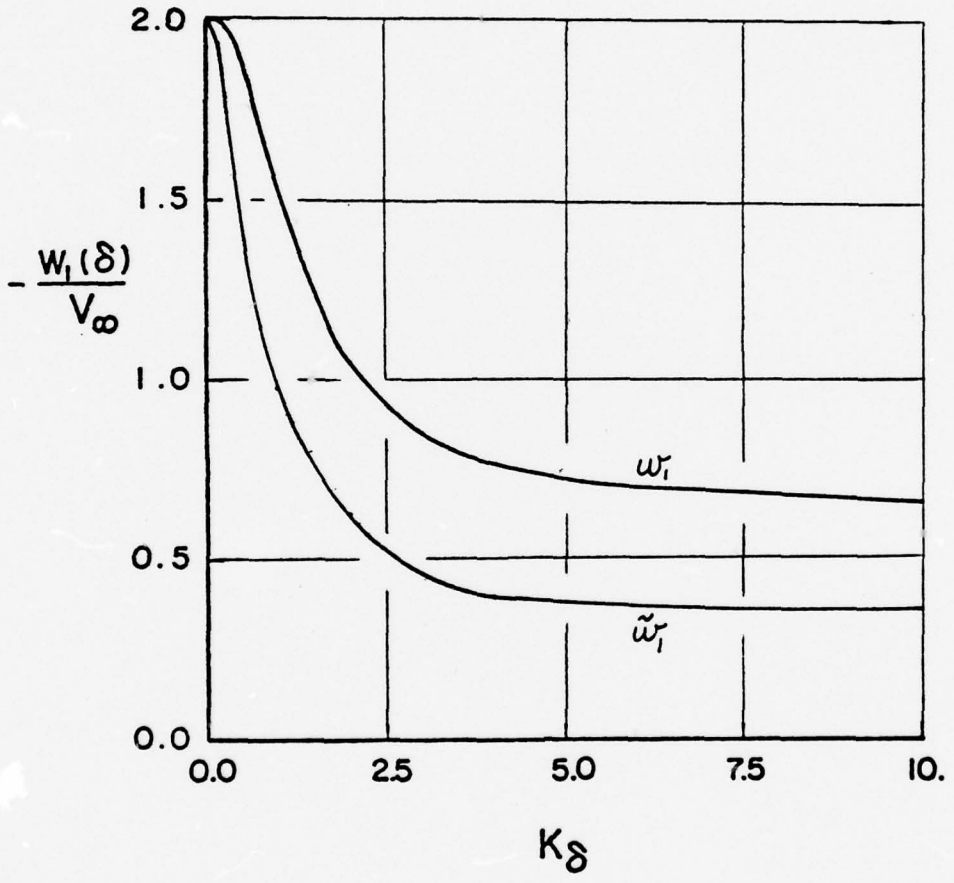

Figure 5.5. Azimuthal Velocity at the Body Surface, $\gamma = 1.4$

the hypersonic limit $K_\delta \to \infty$, $w_1(\delta)/V_\infty$ becomes asymptotic to the value 0.659 for $\gamma = 1.4$. The corresponding angle-of-attack contribution, $\tilde{w}_1(\delta)/V_\infty$, discussed in Section 7, is shown in Fig. 5.5 for comparison.

5.6 Evaluation of the Approximate Analysis

Let the first approximation for the integral equation (4.35) be denoted by $u_1^{(0)}$, which is given by equation (5.7). Then the integral equation (4.35) can be written, for small angles, as

$$u_1 = u_1^{(0)} + u_1^{(c)} \quad , \tag{5.18}$$

where

$$u_1^{(c)}(\theta) \equiv \frac{1}{\sin^2\theta} \int_\beta^\theta \sin^3\theta \left(\int_\beta^\theta \frac{H_1(\theta)}{\sin\theta}\, d\theta \right) d\theta \tag{5.19a}$$

$$\simeq \frac{1}{\theta^2} \int_\beta^\theta \theta^3 \left(\int_\beta^\theta \frac{H_1(\theta)}{\theta}\, d\theta \right) d\theta \tag{3.19b}$$

$$H_1(\theta) = Au_1'' + B \cot\theta\, u_1' + cu_1 \tag{5.20}$$

Consider now an approximate evaluation of the correction function $u_1^{(c)}$. Towards this end we utilize the well-known convergent iteration procedure for Voltera-type integral equations. The first step is to substitute the first approximation $u_1^{(0)}$ into $H_1(\theta)$ and then evaluate $u_1^{(c)}$. Expression (5.7) for $u_1^{(0)}$ is fairly complicated and does not lend itself to a simple analytical evaluation of $u_1^{(c)}$. Figure 5.2 shows, however, that $u_1^{(0)}(\theta)$ can be approximated by the simple formula

$$\frac{u_1^{(0)}}{V_\infty \delta} \simeq \left(\frac{\delta}{\theta}\right)^2 G(\theta, K_\delta) \tag{5.21a}$$

where $G(\theta, K_\delta)$ is a slowly varying function of θ and K_δ, being approximately unity. It now follows approximately that

$$\frac{u_1'^{(0)}}{V_\infty} = \frac{v_1^{(0)}}{V_\infty} \simeq -2 \left(\frac{\delta}{\theta}\right)^3 G \tag{5.21b}$$

$$\frac{u_1''(0)}{V_\infty} \simeq 6 \frac{\delta^3}{\theta^4} \; G \tag{5.21c}$$

since G is nearly a constant. Again it may be verified that expression (5.21b) gives a reasonable approximation to Fig. 5.3.

Substitution of expression (5.21) into (5.20) and than (5.19b) yields

$$u_1^{(c)}(\theta) \simeq u_1^{(0)}(\theta) \int_\beta^\theta \theta^3 \left(\int_\beta^\theta \left[\frac{6A}{\theta^5} - \frac{2B}{\theta^5} + \frac{C}{\theta^3} \right] d\theta \right) d\theta \tag{5.22}$$

In the evaluation of A, B, and C, given by equation (4.29), we set $a_o^2(\theta) \simeq a_o^2(\delta)$ since $a_o^2(\theta)$ varies by only a few percent over the shock layer. With the approximations (5.2a,b) we now get, for small angles, and with $z \equiv \theta/\delta$,

$$A \simeq Nz^2 \left(1 - \frac{1}{z^2}\right)^2 \tag{5.23a}$$

$$B \simeq N \left(1 - \frac{1}{z^2}\right) \left[2 + (\gamma-1) \, Nz^2 \left(1 - \frac{1}{z^2}\right)^2 \right] \tag{.23b}$$

$$C \simeq - (\gamma-1) \, N^2 \frac{z^2}{\theta^2} \left(1 - \frac{1}{z^2}\right)^2 \tag{5.23c}$$

where

$$N \equiv \frac{V_\infty^2 \delta^2}{a_o^2(\beta)} \quad \frac{2\sigma^2}{(\sigma^2-1)(2\sigma^2+\gamma-1)} \tag{5.24}$$

where $\sigma \equiv \beta/\delta$, given by (5.15). With the formulas (5.23), the integral in (5.22) can be evaluated. We obtain

$$\frac{u_1^{(c)}(\theta)}{Nu_1^{(0)}(\theta)} \simeq -4\ln\left(\frac{\sigma}{z}\right) + \frac{(\sigma^2-z^2)}{2}\left(3 + \frac{5}{3\sigma^2z^2}\right)$$

$$+ (\sigma^4-z^4)\left(-\frac{3}{4\sigma^2} + \frac{1}{\sigma^4} - \frac{5}{12\sigma^6}\right)$$

$$+ (\gamma-1)N\left[2\ln\left(\frac{\sigma}{z}\right) - \frac{(\sigma^2-z^2)}{4}\left(3 + \frac{7}{3\sigma^2z^2}\right)\right. \qquad (5.25)$$

$$\left. + (\sigma^4-z^4)\left(\frac{3}{8\sigma^2} - \frac{1}{2\sigma^4} + \frac{7}{24\sigma^6} - \frac{1}{16\sigma^8} + \frac{1}{16\sigma^4z^4}\right)\right]$$

At the shock, $z = \sigma$, the correction vanishes, $u_1^{(c)}(\beta) = 0$. The largest correction occurs at the body surface, $z = 1$. Then we have

$$\frac{u_1^{(c)}(\delta)}{Nu_1^{(0)}(\delta)} \simeq -4\ln\sigma + \frac{(\sigma^2-1)}{4}\left(3 + \frac{13}{3\sigma^2} + \frac{7}{3\sigma^4} - \frac{5}{3\sigma^6}\right) \qquad (5.26)$$

$$+ (\gamma-1)N\left[2\ln\ - \frac{(\sigma^2-1)}{8}\left(3 + \frac{31}{6\sigma^2} + \frac{7}{6\sigma^4} - \frac{11}{6\sigma^6} + \frac{1}{2\sigma^8}\right)\right]$$

The correction factor $u_1^{(c)}(\delta)/u_1^{(0)}(\delta)$ is shown in Fig. 5.6 as a function of K_δ and $\gamma = 1.4$. In the hypersonic limit, $K_\delta = \infty$, the correction factor is approximately -0.0073, and thus the error in the first approximation is about one percent or less. As K_δ decreases, the correction becomes slightly more negative, being approximately -0.015 at $K_\delta = 1.7$. As K_δ decreases further, the correction factor increases from the minimum negative value and becomes zero at $K_\delta \simeq 1$. Further decreases in K_δ give a rapid increase in the correction factor, becoming 0.75 in the limit $K_\delta = 0$ which corresponds to linearized theory.

In the hypersonic flow range, we can expect the first approximation, obtained by neglecting $u_1^{(c)}$, to be very accurate. In fact, this is true

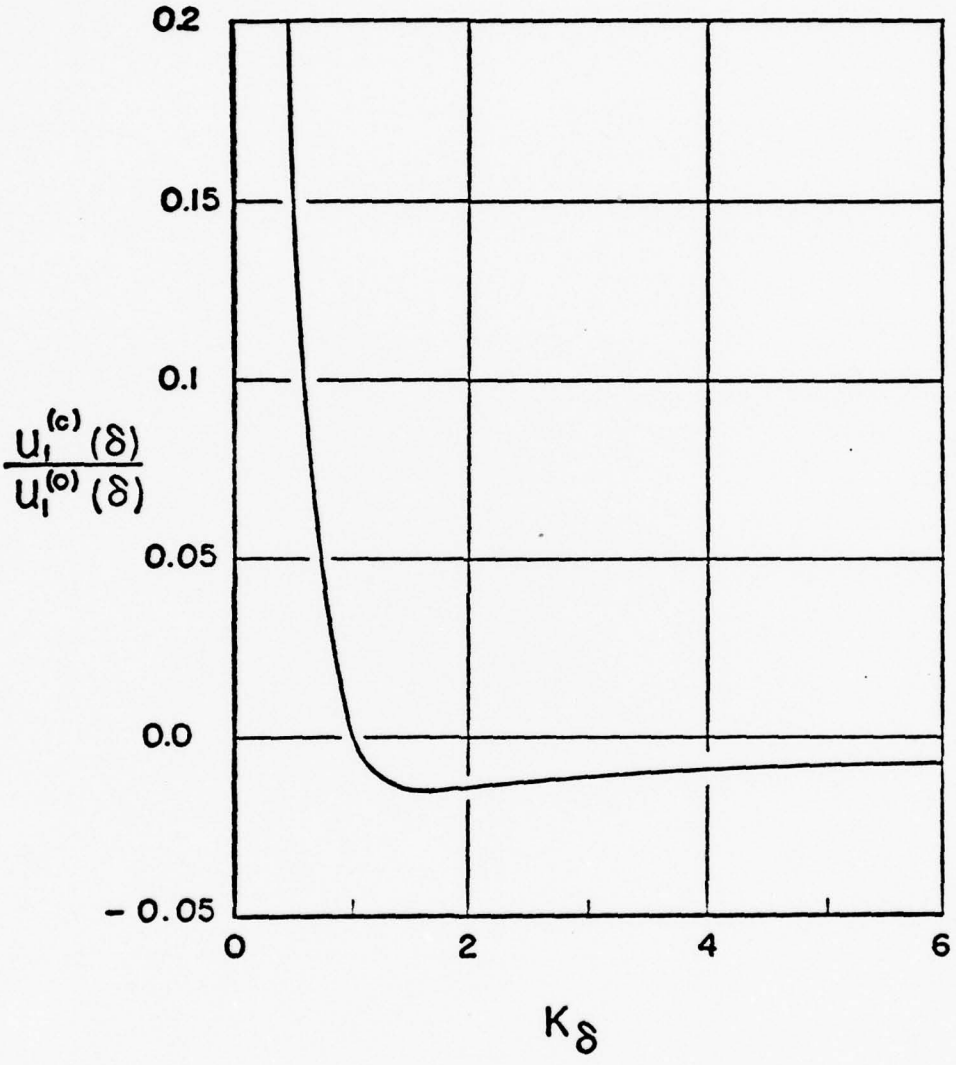

Figure 5.6. Correction Velocity Ratio, $\gamma = 1.4$

when $K_\delta \gtrsim 1$. When $K_\delta < 1$, the first approximation is less accurate. We note, however, that the correct limiting results for $K_\delta = 0$, which correspond to the limiting case of linearized theory, are recovered. This is true because the perturbation u_1 itself vanishes when $\delta \to 0$ and also because the surface boundary condition $v_1(\delta) = -2V_\infty$ is enforced on the first approximation itself (which produces the first approximation for g). The surface boundary condition is always exactly enforced. Thus, although the linearized limit $K_\delta = 0$ is recovered, the approach to the linearized limit is in error. Because the results are correct at $K_\delta = 0$ and very nearly correct at $K_\delta = 1$, the error in the range $0 < K_\delta < 1$, while greater than for $K_\delta > 1$, is less than that indicated in Fig. 5.6.

The above observations are born out by the results of Doty and Rasmussen [13] for hypersonic flow past a circular cone at angle of attack. Their approximate analysis was analogous to the present analysis, but the results could be compared extensively with well-known tabulated results. The agreement was very good. Thus, whereas extensive tabulated results for the elliptic cone do not exist as they do for the circular cone at angle of attack, the above error analysis and the experience of Doty and Rasmussen justify confidence in the present analysis.

6. SURFACE PRESSURE ON THE ELLIPTIC CONE

6.1 Surface Perturbation Pressure Coefficient

The pressure on the surface of the cone is given by (for $\alpha = 0$)

$$p(\theta_c,\phi) = p_o(\theta_c) + \varepsilon p_1(\theta_c) \cos 2\phi + O(\varepsilon^2) \tag{6.1}$$

where

$$\theta_c = \delta - \varepsilon\cos 2\phi + O(\varepsilon^2) \tag{6.2}$$

Transferring the expression (6.1) to the basic cone gives

$$p(\theta_c,\phi) = p_o(\delta) + \varepsilon\left[p_1(\delta) - \left(\frac{dp_o}{d\theta}\right)_\delta \right] \cos 2\phi + O(\varepsilon^2) \tag{6.3}$$

At the cone surface, the gradient of the basic pressure, p_o, vanishes since $v_o(\delta) = 0$, that is,

$$\left(\frac{dp_o}{d\theta}\right)_\delta = - \rho_o(\delta)\, v_o(\delta) \left[u_o + \frac{dv_o}{d\theta} \right]_\delta = 0 \tag{6.4}$$

Hence we have

$$p(\theta_c,\phi) = p_o(\delta) + \varepsilon p_1(\delta) \cos 2\phi + O(\varepsilon^2) \tag{6.5}$$

The pressure coefficient, C_p, is defined by

$$C_p = \frac{\frac{p}{p_\infty} - 1}{\frac{\gamma}{2} M_\infty^2} \tag{6.6}$$

Thus we can write

$$C_p = C_{p_o} + \varepsilon C_{p_1} \cos 2\phi + O(\varepsilon^2) \tag{6.7}$$

where

$$C_{p_o} \equiv \frac{\frac{p_o(\delta)}{p_\infty} - 1}{\frac{\gamma}{2} M_\infty^2} \tag{6.8a}$$

$$C_{p_1} \equiv \frac{2p_1(\delta)}{\gamma p_\infty M_\infty^2} \qquad (6.8b)$$

The pressure perturbation is given by equation (4.8), and since $v_o(\delta) = 0$, we have

$$p_1(\delta) = - \rho_o(\delta)\, u_o(\delta)\, u_1(\delta) + p_o(\delta)\, F_1 \qquad (6.9)$$

Using the previous results for the first approximation, we obtain the hypersonic similarity form

$$\frac{C_{p_1}}{\delta} = \frac{2N}{K_\delta^2} \frac{p_o(\delta)}{p_\infty} \left[\frac{g}{\sigma^3} - \frac{a_o^2(\beta)}{a_o^2(\delta)} \frac{u_1(\delta)}{V_\infty \delta} \right] \qquad (6.10)$$

where

$$\frac{p_o(\delta)}{p_\infty} = 1 + \frac{\gamma}{2} K_\delta^2 \left(\frac{C_{p_o}}{\delta^2} \right) \qquad (6.11)$$

and N is given by (5.24). From an analysis of the basic cone flow [11,12,13] we have

$$\frac{a_o^2(\delta)}{a_o^2(\beta)} = 1 + \frac{(\gamma-1)\, \sigma^2 \left[\ln \sigma^2 + \frac{1}{\sigma^2} - 1 \right]}{(\sigma^2 - 1)(2\sigma^2 + \gamma - 1)} \qquad (6.12a)$$

$$\frac{C_{p_o}}{\delta^2} = 1 + \frac{\sigma^2 \ln \sigma^2}{\sigma^2 - 1} \qquad (6.12b)$$

Figure 6.1 shows C_{p_1}/δ plotted as a function of K_δ for $\gamma = 1.4$. For $K_\delta = 0$, we get $C_{p_1}/\delta = -2$, in agreement with linearized theory. In the hypersonic limit, $K_\delta = \infty$, C_{p_1}/δ approaches the value -3.811. Thus in the hypersonic limit, the surface pressure coefficient approaches the form

$$\frac{C_p}{\delta^2} = 2.094 - 3.811 \frac{\varepsilon}{\delta} \cos 2\phi + O(\varepsilon^2) \qquad (6.13)$$

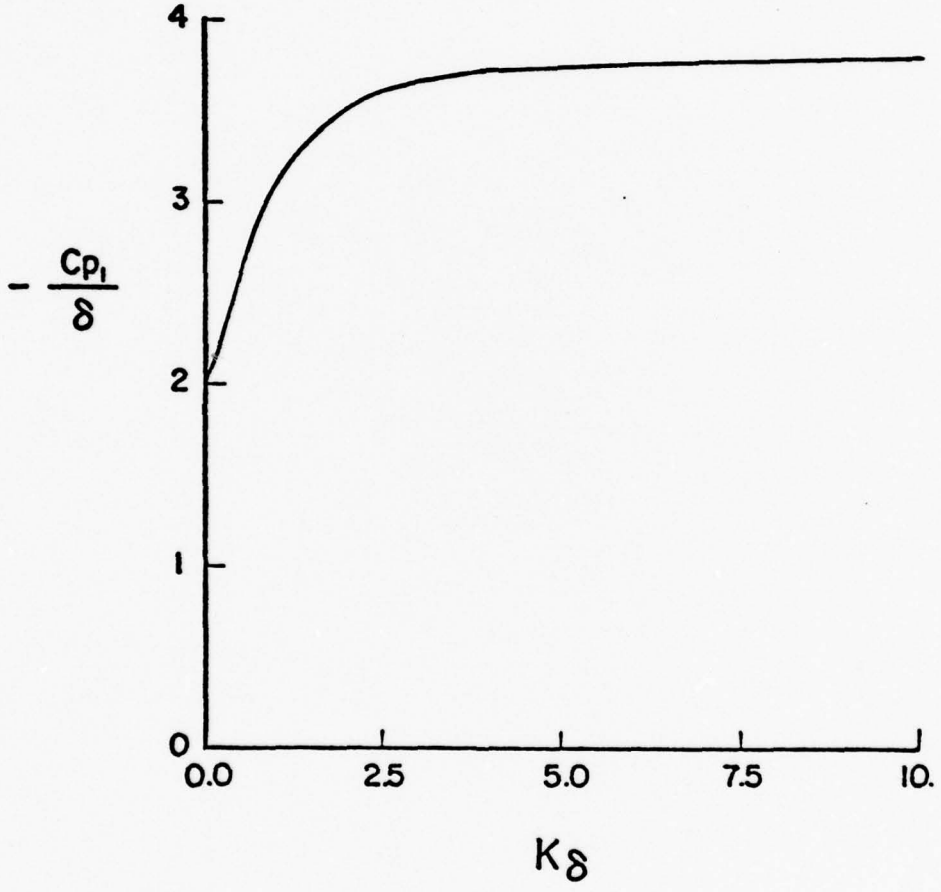

Figure 6.1. Perturbation Pressure Coefficient on the Body Surface

6.2 Comparison with Experiment

Surface pressures were measured on two different elliptic cone models, each at free stream Mach numbers 3.09 and 6.0, by Zakkay and Visich [16]. The geometric properties of these models were as follows:

Model I	Model II
$a = 0.2555$	$a = 0.2256$
$b = 0.3562$	$b = 0.4034$
$e = 0.320$	$e = 0.523$
$\theta_m = 16.36°$	$\theta_m = 15.56°$
$\varepsilon/\delta = 0.155$	$\varepsilon/\delta = 0.266$
$\delta = 16.64° = 0.2904$ rad	$\delta = 16.28° = 0.2841$ rad

These two models have the same cross sectional areas for the same station along the elliptic-cone axis. A circular cone with the same cross sectional area has a semi-vertex angle of 16.79°. The experimental data are compared with the results of the present analysis and also with the analysis of Martellucci [5]. Martellucci used an extension of the so-called linearized characteristics method. This method essentially uses the first-order perturbation equations utilized in the present analysis, but takes a finite number of terms in a Fourier series expansion to represent the shape of this surface. Martellucci used the first six terms. (In view of the fact that the Fourier coefficients for an ellipse decrease in magnitude like powers of the eccentricity, e, as seen in equation (2.6), it would seem that a higher-order theory should be utilized to accommodate the higher-order Fourier coefficients. In this sense, the linearized-characteristics method

does not seem to be entirely rational, at least for the ellipse.) The perturbation equations were integrated numerically by Martellucci, but the general results corresponding to the present analysis were not obtained.

Figure 6.2 shows the pressure distribution on one quadrant of model I for the elliptic cone for $M_\infty = 6.0$, which corresponds to $K_\delta = 1.747$. The present results agree very well with the data on the major and minor rays ($\phi = 90°$ and $180°$), but give pressures that are too large in between. The overall agreement is good considering that the perturbation theory should be strictly valid when $\varepsilon << \delta$, and this condition is met only marginally. The results of Martellucci give slightly better agreement with the data, but probably not enough to justify the numerical computational effort.

Figure 6.3 shows pressure-distribution data on model II for $M_\infty = 6.0$, which corresponds to $K_\delta = 1.724$. This model is substantially more eccentric than model I, and the condition $\varepsilon << \delta$ is certainly not satisfied. Nevertheless, fairly good agreement with the present analysis definitely represents the overall trends of the data. The results of Martellucci do not appear to give substantially better overall agreement with the data.

Figure 6.4 shows the pressure-distribution data on model I for the smaller Mach number, $M_\infty = 3.09$, for which $K_\delta = 0.900$. Again the present results give good agreement with the data on the semi-major ray, but the data are lower otherwise. The overall agreement does not seem to be quite as good as for the higher Mach number $M_\infty = 6.0$, which might be partially expected on the grounds that the approximate

analysis is less accurate at $K_\delta = 0.900$ than for $K_\delta = 1.747$. The results of Martellucci give a little better agreement with the data between the major and minor rays.

Figure 6.5 shows the pressure-distribution data on model II for $M = 3.09$, for which $K_\delta = 0.888$. The agreement with the present analyses is fairly good near the major and minor rays, but poor in between. Again, for this large value of eccentricity, higher-order perturbation terms are probably required. The linearized-characteristics method used by Martellucci picks up higher-order harmonics in Fourier representation of the ellipse and thus shows somewhat better agreement with the data between the major and minor rays. In view of the large value of ε, however, there are probably higher-order perturbation terms that are of the same order of magnitude as the higher-order Fourier harmonics.

6.3 Drag on the Elliptic Cone

The pressure force on a finite-length elliptic cone is given by

$$\vec{F} = -\int\int_S p(\theta_c)\, \hat{n}\, dS \tag{6.14}$$

where S is the area of the slant face, and

$$\theta_c = \delta - \varepsilon \cos 2\phi + O(\varepsilon^2) \tag{6.15a}$$

$$\hat{n} = \hat{e}_\theta - \frac{2\varepsilon \sin 2\phi}{\sin \delta}\, \hat{e}_\phi + O(\varepsilon^2) \tag{6.15b}$$

$$dS = r \sin \theta_c\, dr\, d\phi + O(\varepsilon^2)$$

$$= z \frac{\tan \theta_c}{\cos \theta_c}\, dz\, d\phi + O(\varepsilon^2) \tag{6.15c}$$

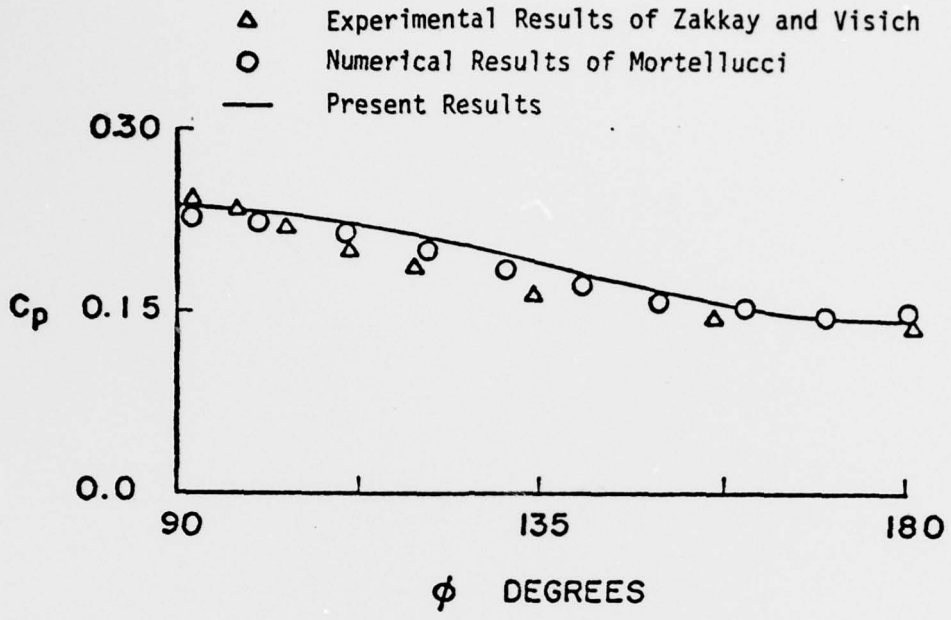

Figure 6.2. Pressure Coefficient on Body Surface
Model I, $M_\infty = 6$, $\gamma = 1.4$

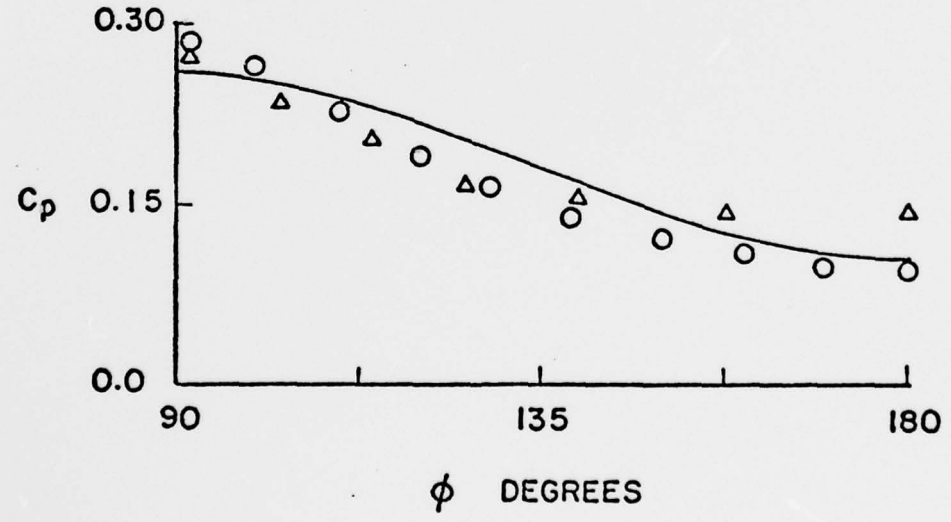

Figure 6.3. Pressure Coefficient on Body Surface
Model II, $M_\infty = 6$, $\gamma = 1.4$

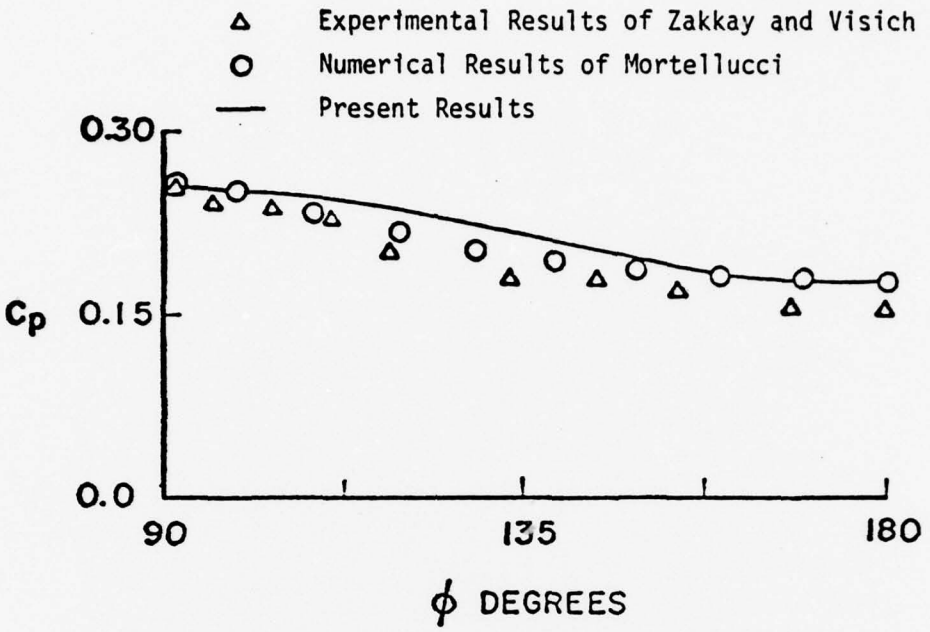

Figure 6.4. Pressure Coefficient on Body Surface
Model I, $M_\infty = 3.09$, $\gamma = 1.4$

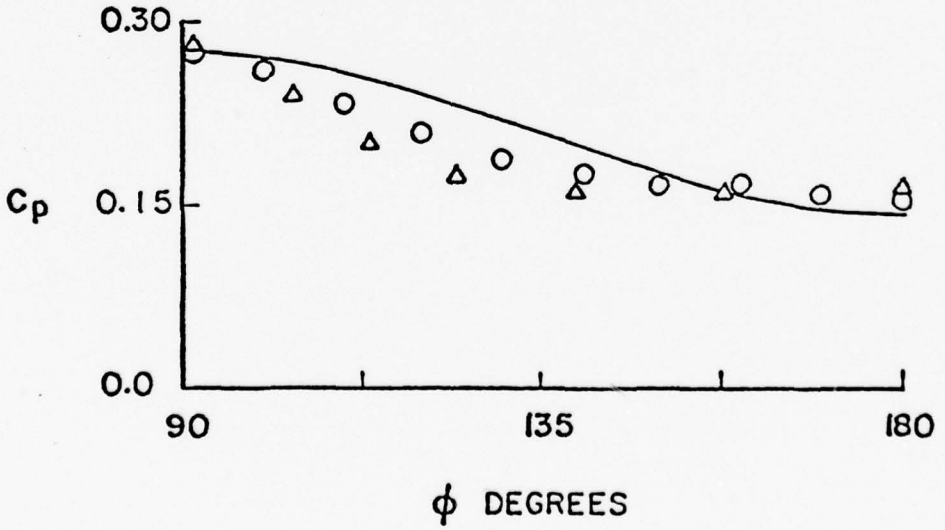

Figure 6.5. Pressure Coefficient on Body Surface
Model II, $M_\infty = 3.09$, $\gamma = 1.4$

$$p(\theta_c) = p_0(\delta) + \varepsilon p_1(\delta) \cos 2\phi + O(\varepsilon^2) \qquad (6.15d)$$

When the integration is carried out in the range $0 \leq \phi \leq 2\pi$ and $0 \leq z \leq H$, where H is the length of the cone axis, we get for the cone drag

$$D \equiv \vec{F} \cdot \hat{e}_z = p_0(\delta)A + O(\varepsilon^2) \quad , \qquad (6.16)$$

where

$$A = \pi H^2 \tan^2 \delta \qquad (6.17)$$

is the base area of the basic cone of semi-vertex angle δ. Thus the drag on the elliptic cone, ignoring terms of order ε^2, is the same as the drag on the basic cone of semi-vertex angle δ having the same length.

7. ELLIPTIC CONE AT ANGLE OF ATTACK

7.1 Superposition of Results

Let the freestream wind be inclined to the axis of the elliptic cone such that the inclination angle, α, is measured in the x-z plane shown in Fig. 2.1. Let the coordinate system remain fixed to the body so that the z-axis is the axis of the cone. The surface boundary conditions remain unchanged. The shock shape can now be represented by [12]

$$\theta_s = \beta + \alpha\tilde{g} \cos \phi - \varepsilon g \cos 2\phi + O(\alpha^2, \alpha\varepsilon, \varepsilon^2) \qquad (7.1)$$

where $\tilde{g}$ is the eccentricity factor associated with angle of attack. We assume α and ε to be small and of the same order of magnitude. Since the first-order perturbation equations and boundary conditions are linear, the angle of attack problem for the circular cone can be superposed with the elliptic-cone solution at zero angle of attack. The subsequent results for the circular-cone angle of attack problem were obtained by Doty [12] and Doty and Rasmussen [13] by an analysis very similar to the foregoing analysis for the elliptic cone. The angle-of-attack shock eccentricity factor was found to have the form

$$\tilde{g} = \frac{3 + 2\sigma^2\left[3 - \frac{4(1+\sigma^2)}{\gamma+1}\right] - \left[\sigma(\sigma^2-1)^{1/2}\right]^{-1} \ln\left[\sigma + (\sigma^2-1)^{1/2}\right]}{5 - 2(1+\sigma^2)\left[1 + \frac{4\sigma^2}{\gamma+1}\right] - \left[\sigma(\sigma^2-1)^{1/2}\right]^{-1} \ln\left[\sigma + (\sigma^2-1)^{1/2}\right]} \qquad (7.2)$$

where σ is given by (5.15) as before. This function is shown in Fig. 5.1.

The first-order expansion for the flow variables outside the vortical layer can be written as

$$u(\theta,\phi) = u_0(\theta) + \alpha\tilde{u}_1(\theta)\cos\phi + \varepsilon u_1(\theta)\cos 2\phi \qquad (7.3a)$$

$$v(\theta,\phi) = v_0(\theta) + \alpha\tilde{v}_1(\theta)\cos\phi + \varepsilon v_1(\theta)\cos 2\phi \qquad (7.3b)$$

$$w(\theta,\phi) = \alpha\tilde{w}_1(\theta)\sin\phi + \varepsilon w_1(\theta)\sin 2\phi \qquad (7.3c)$$

$$\rho(\theta,\phi) = \rho_0(\theta) + \alpha\tilde{\rho}_1(\theta)\cos\phi + \varepsilon\rho_1(\theta)\cos 2\phi \qquad (7.3d)$$

$$p(\theta,\phi) = p_0(\theta) + \alpha\tilde{p}_1(\theta)\cos\phi + \varepsilon p_1(\theta)\cos 2\phi \qquad (7.3e)$$

The variables with the tilde notation pertain to the angle of attack solution past a circular cone.

7.2 Pressure on the Body Surface

The pressure on the body surface is given by

$$p(\theta_c,\phi) = p_0(\delta) + \alpha\tilde{p}_1(\delta)\cos\phi + \varepsilon p_1(\delta)\cos 2\phi \qquad (7.4)$$

where

$$\tilde{p}_1(\delta) = -\rho_0(\delta)\,u_0(\delta)\tilde{u}_1(\delta) + p_0(\delta)\,\tilde{F}_1 \qquad (7.5)$$

$$\tilde{F}_1 \equiv +\gamma V_\infty^2\beta(1-\tilde{g})(1-\xi_0)^2/a_0^2(\beta) \qquad (7.6)$$

$$\frac{\tilde{u}_1(\delta)}{V_\infty\delta} = -2 + \frac{(1-\tilde{g})}{\sigma^3}\left[\frac{4\sigma^5}{\gamma+1} + \sigma^3 - \frac{\sigma}{2} + 1 - \frac{\ln(\sigma+\sqrt{\sigma^2-1})}{2\sqrt{\sigma^2-1}}\right] \qquad (7.7)$$

which is analogous to expression (6.9). In terms of the pressure coefficient, we have

$$C_p = C_{p_0} + \alpha\tilde{C}_{p_1}\cos\phi + \varepsilon C_{p_1}\cos 2\phi \qquad (7.8)$$

where

$$\frac{\tilde{C}_{p_1}}{\delta} = \frac{2N}{K_\delta^2} \frac{p_o(\beta)}{p_\infty} \frac{p_o(\delta)}{p_o(\beta)} \left[\frac{(1-\tilde{g})}{\sigma^3} - \frac{a_o^2(\beta)}{a_o^2(\delta)} \frac{\tilde{u}_1(\delta)}{V_\infty \delta} \right] \quad (7.9)$$

In the calculations of Doty [12] and Doty and Rasmussen [13], the ratios $p_o(\delta)/p_o(\beta)$ and $a_o^2(\beta)/a_o^2(\delta)$ were set equal to unity consistent with their "constant-density" approximation.

The angle of attack perturbation pressure coefficient given by (7.9) is shown in Fig. 7.1 When $K_\delta = 0$, the limiting result of linearized theory is recovered, $\tilde{C}_{p_1}/\delta = -4$. When $K_\delta = \infty$, the limiting hypersonic value is $\tilde{C}_{p_1}/\delta = -4.0836$. Near $K_\delta = 1$, there is a small dip in the curve. As K_δ approaches zero, there is a small overshoot in the curve which does not occur in the exact theory. Over the range of K_δ, the value of $\tilde{C}_{p_1}/\delta$ does not differ greatly from -4. In the hypersonic limit, $K_\delta = \infty$, we can write

$$\frac{C_p}{\delta^2} = 2.094 - 4.084 \left(\frac{\alpha}{\delta}\right) \cos\phi - 3.811 \left(\frac{\varepsilon}{\delta}\right) \cos 2\phi \quad (7.10)$$

correct to first order in α and ε. Expression (7.10) indicates that α/δ and ε/δ should be sufficiently small in order for the perturbation analysis to be valid.

7.3 Comparison with Other Results

The present results for surface pressure at $M_\infty = 6$ and angles of attack of $\alpha = 5°$ and $10°$ are shown in Figs. 7.2 and 7.3 for models I and II. The results of Martellucci are shown for comparison together with the experimental data of Zakkay and Visich for $\alpha = 10°$, which is a large enough angle of attack to make for a demanding comparison. The present results agree well with Martelluci for both models for $\alpha = 5°$, the worst agreement being on the leeward ray,

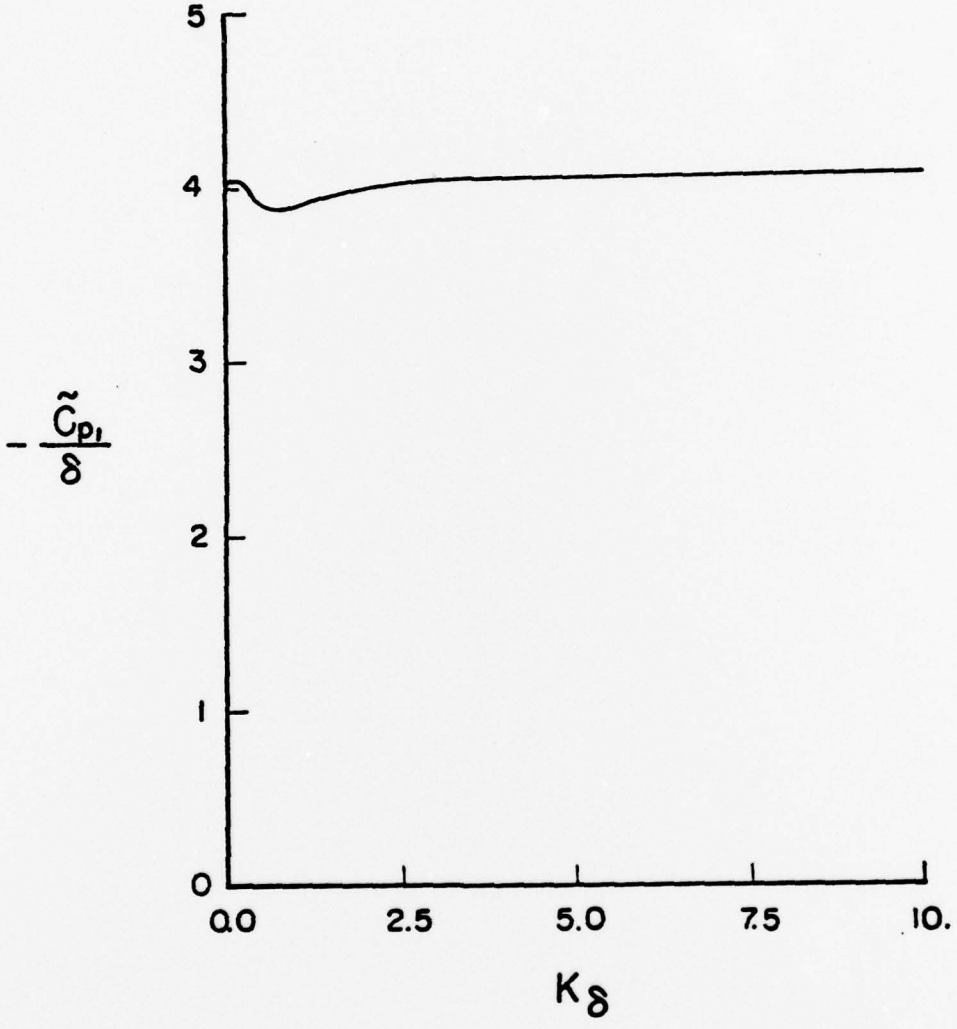

Figure 7.1. Angle-of-Attack Perturbation Surface Pressure Coefficient, $\gamma = 1.4$

$\phi = 0°$. For $\alpha = 10°$, the two results are in fair agreement for the small-eccentricity ellipse, model I in Fig. 7.2, except near the leeward ray of the elliptic cone. For the large-eccentricity ellipse at $\alpha = 10°$, model II in Fig. 7.3, agreement between the two results is good only near the windward ray. For model II at $\alpha = 10°$, the combined large values of $\alpha/\delta = 0.607$ and $\varepsilon/\delta = 0.270$ render the first-order perturbation theory invalid, especially near the leeward ray where the separate perturbations are additive.

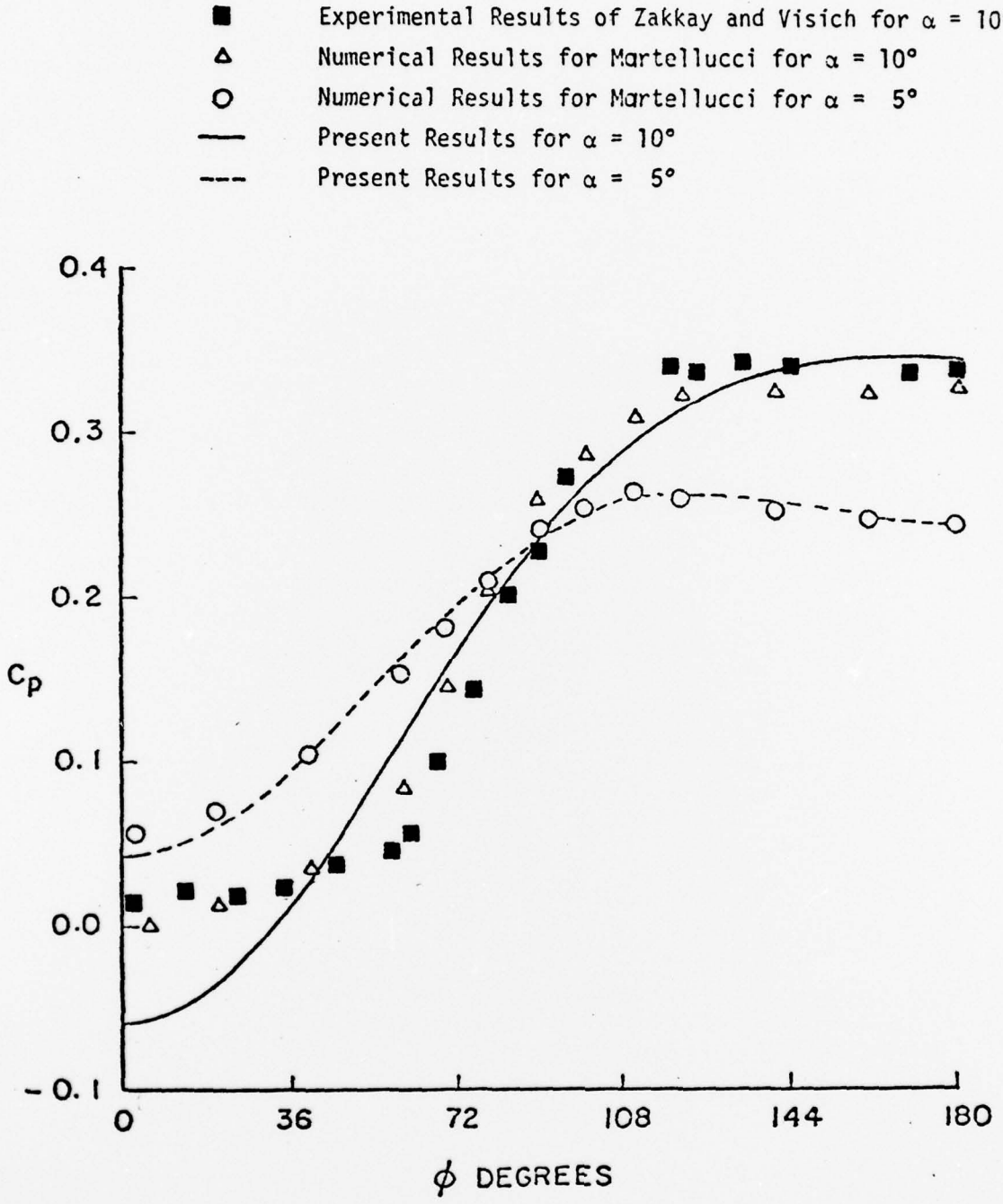

Figure 7.2. Comparison of Surface Pressure with Martellucci's Results, Model I, $M_\infty = 6$, $\gamma = 1.4$

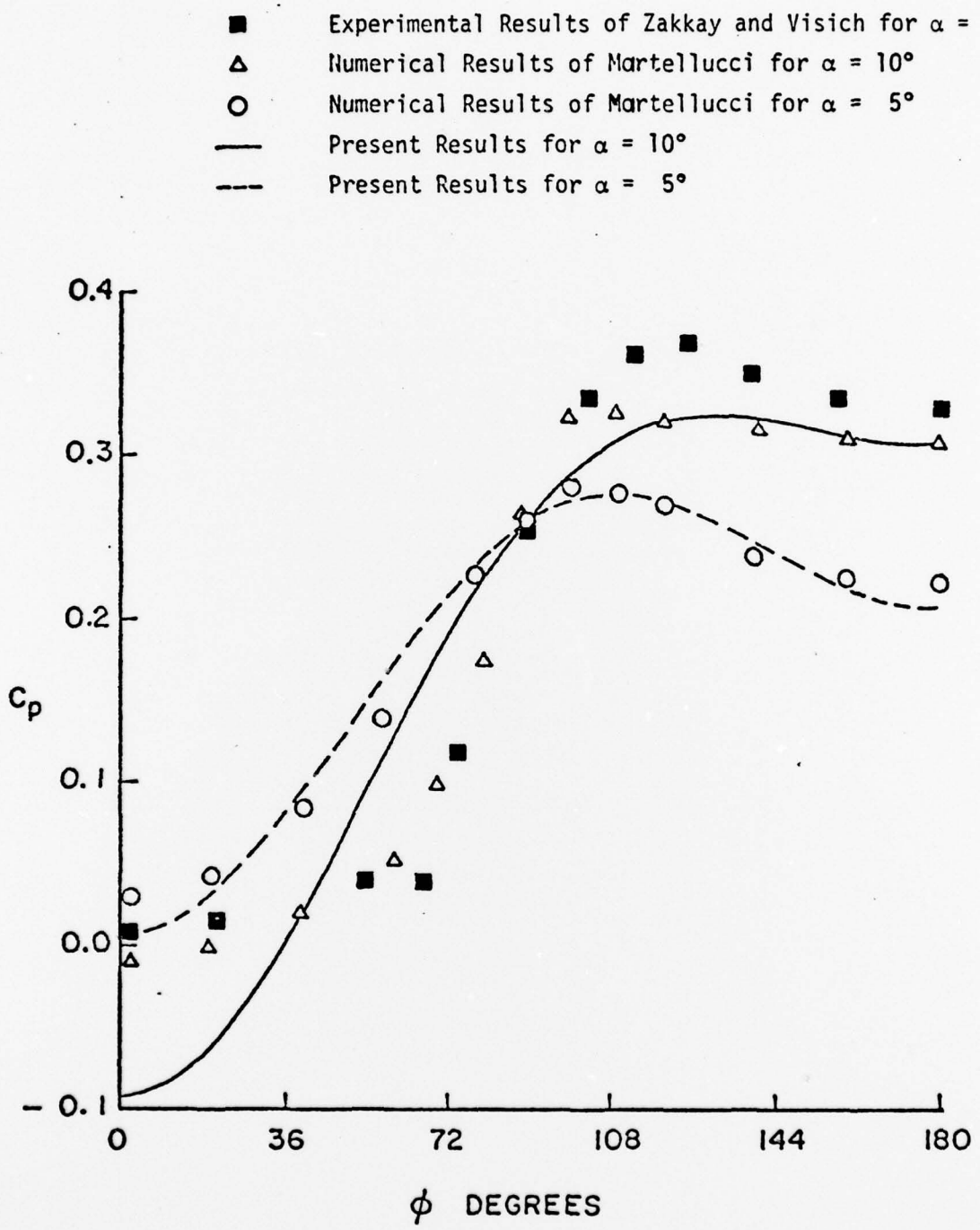

Figure 7.3. Comparison of Surface Pressure with Martellucci's Results, Model II, $M_\infty = 6$, $\gamma = 1.4$

7.4 Normal Force on the Elliptic Cone

The normal-force on the cone is found to be

$$\vec{F}\cdot\hat{e}_x = C_{N_\alpha}\,\alpha\,\frac{\gamma}{2}M_\infty^2 p_\infty A + O(\alpha^2,\varepsilon^2,\alpha\varepsilon) \tag{7.11}$$

where $\vec{F}$ is defined by (6.14), $A \equiv \pi H^2 \tan^2\delta$ is the base area of the basic cone of semi-vertex angle δ, and

$$C_{N_\alpha} = -\frac{1}{2}\frac{\tilde{C}_{P_1}}{\delta} \tag{7.12}$$

is the α- derivative of the normal-force coefficient.

The moment about the cone vertex is

$$\vec{M} = -\int\int_S p(\theta_c)\,\vec{r}\times\hat{n}_c\,dS \tag{7.13}$$

Evaluation of this integral gives

$$\vec{M} = \hat{e}_y\left[C_{M_\alpha}\,\alpha\,\frac{\gamma}{2}M_\infty^2 p_\infty HA\right] + O(\alpha^2,\varepsilon^2,\varepsilon\alpha) \tag{7.14}$$

where

$$C_{M_\alpha} = \frac{2}{3}C_{N_\alpha} = -\frac{1}{3}\frac{\tilde{C}_{P_1}}{\delta} \tag{7.15}$$

is the α- derivative of the moment coefficient.

For completeness, we can rewrite the drag on the elliptic cone, (6.16), in terms of an axial-force coefficient. If the base pressure is reckoned as p_∞, then we have

$$\vec{F}\cdot\hat{e}_z = C_A\,\frac{\gamma}{2}M_\infty^2 p_\infty A + (\alpha^2,\varepsilon^2,\alpha\varepsilon) \tag{7.16}$$

where

$$C_A = C_{p_o} = \left(\frac{\tilde{C}_{p_o}}{\delta^2}\right)\delta^2 \tag{7.17}$$

and C_{p_o} is given by (6.12b).

The ratios $\frac{\tilde{C}_{p_1}}{\delta}$ and $\frac{\tilde{C}_{p_o}}{\delta^2}$ depend only on K_δ and γ. They are insensitive to K_δ when K_δ is large. Thus when K_δ is large, that is, for hypersonic flow, the main effect of the cone cross-section shape is determined from δ. For slender cones (small θ_m) we have from (2.3a) and (2.8a) the alternative forms

$$\begin{aligned} \delta &= \sqrt{ab}\,[1 + O(e^2)] \\ \delta &= b\sqrt{1-e}\,[1 + O(e^2)] \end{aligned} \tag{7.18}$$

The cross-section area of an ellipse is proportional to the product ab. Hence when the cross-section area is held fixed, the force coefficients are independent of the eccentricity e when terms of order e^2 are neglected.

On the other hand, when b is held fixed, then δ varies with the eccentricity to the first power. The normal force and moment are independent of δ when K_δ is large, but C_A decreases with increasing e when b is held fixed. Thus the lift-drag ratio increases when b is held fixed and e increases.

8. CONCLUDING REMARKS

General flow field results for the hypersonic flow past an elliptic cone have been obtained. The results are valid for large Mach numbers and small stream deflections such that the hypersonic similarity parameter, $K_\delta \equiv M_\infty \delta$, is fixed in the limiting process. The results are more accurate for large K_δ ($K_\delta \gtrsim 1$), but the proper linearized theory result is recovered when $K_\delta \to 0$. The ellipse eccentricity factor, e, in the analysis must be small in the strict sense that $\varepsilon/\delta << 1$. Comparison with experimental results indicates that ε/δ need not be very much less than unity, but merely moderately less than unity, for acceptable engineering results. In addition, the angle of attack should be such that $\alpha/\delta << 1$ in the strict perturbation sense. An important feature of the analysis is that the basic circular cone angle, δ, has been well defined in terms of the geometric properties of the elliptic cone.

The methodology of this analysis can be extended to other cross-section shapes. Each term in a Fourier expansion of the cross-section shape can be handled in an analogous manner and accurate, approximate analytic results obtained. Strictly speaking, however, the cross-section shapes should deviate only slightly from a circular cone in order for the perturbation analysis to be valid. Moreover, successive Fourier coefficients should not decrease in powers of the basic expansion parameter, for then corresponding terms of higher-order perturbations become equally important.

REFERENCES

1. Mascitti, V.R. "Calculation of Linearized Supersonic Flow Over Slender Cones of Arbitrary Cross Section." NASA TN D=6818, July, 1972.

2. Van Dyke, M.D. "The Slender Elliptic Cone as a Model for Nonlinear Supersonic Flow Theory." Journal of Fluid Mechanics, Vol. 1, Part 1, 1956, pp. 1-15.

3. Ferri, A., Ness, N., and Kaplita, T. "Supersonic Flow Over Conical Bodies Without Axial Symmetry." Journal of the Aeronautical Sciences, Vol. 20, No. 8, 1953, pp. 563-571.

4. Vaglio-Laurin, R. and Van Dyke, M.D. "A Discussion of Higher-Order Approximations for the Flow Field About a Slender Elliptic Cone." Journal of Fluid Mechanics, Vol. 3, Part 6, 1958, pp. 638-644.

5. Martellucci, A. "An Extension of the Linearized Characteristics Method for Calculating the Supersonic Flow Around Elliptic Cones." J. Aero. Sci., Vol. 27, No. 9, 1960, pp. 667-674.

6. Chapkis, R.T. "Hypersonic Flow Over an Elliptic Cone: Theory and Experiment." Journal of the Aeronautical Science, Vol. 28, No. 11, 1961, pp. 844-854.

7. Stocker, P.M. and Mauger, F.E. "Supersonic Flows Past Cones of General Cross Section." Journal of Fluid Mechanics, Vol. 13, Part 3, 1962, pp. 383-399.

8. Babenko, K.I., Voskresenskiy, Lyubimov, A.N., and Rusanov, V.V. "Three Dimensional Flow of an Ideal Gas Past Smooth Bodies." NASA TT F-380, April, 1966.

9. Kaattari, G. "Method for Predicting Pressures on Elliptic Cones at Supersonic Speeds." NASA TN D-5952, August, 1970.

10. Pottsepp, L. "Inviscid Hypersonic Flow Over Unyawed Circular Cones." J. Aero. Sci., Vol. 27, No. 7, 1960. p.558.

11. Rasmussen, M.L. "On Hypersonic Flow Past an Unyawed Cone." AIAA Journal, Vol. 5, No. 8, 1967, pp. 1495-1497.

12. Doty, R.T. "Hypersonic Flow Past an Inclined Cone." M.S. Thesis, Aerospace, Mechanical and Nuclear Engineering, University of Oklahoma, 1972.

13. Doty, R.T. and Rasmussen, M.L. "Approximation for Hypersonic Flow Past an Inclined Cone." AIAA Journal, Vol. 11, No. 9, 1973, pp. 1310-1315.

14. Cheng, H.K. "Hypersonic Flows Past a Yawed Circular Cone and Other Pointed Bodies." Journal of Fluid Mechanics, Vol. 20, 1962, pp. 169-191.

15. Melnik, R.E. "Vortical Singularities in Conical Flow." AIAA Journal, Vol. 5, No. 4, 1967, pp. 631-637.

16. Zakkay, V. and Visich, M., Jr. "Experimental Pressure Distribution on Conical Elliptic Bodies at M_∞ = 3.09 and 6.0." Polytechnic Institute of Brooklyn, PIBAL Report No. 467, March 1959.

SECURITY CLASSIFICATION OF THIS PAGE *(When Data Entered)*

REPORT DOCUMENTATION PAGE	READ INSTRUCTIONS BEFORE COMPLETING FORM
1. REPORT NUMBER: AFOSR-TR- 79-0473	2. GOVT ACCESSION NO. / 3. RECIPIENT'S CATALOG NUMBER
4. TITLE *(and Subtitle)*: HYPERSONIC FLOW PAST A SLENDER ELLIPTIC CONE	5. TYPE OF REPORT & PERIOD COVERED: Final Scientific ~~PART I~~
	6. PERFORMING ORG. REPORT NUMBER
7. AUTHOR(s): Hsiung Ming Lee Maurice L Rasmussen	8. CONTRACT OR GRANT NUMBER(s): AFOSR-77-3468
9. PERFORMING ORGANIZATION NAME AND ADDRESS: Aerospace, MECHANICAL & Nuclear Engineering University of Oklahoma Norman, Oklahoma 73019	10. PROGRAM ELEMENT, PROJECT, TASK AREA & WORK UNIT NUMBERS: 2301/A6 / 61102F
11. CONTROLLING OFFICE NAME AND ADDRESS: AFOSR/NP Bolling AFB Wash DC 20332	12. REPORT DATE: Nov 1978 13. NUMBER OF PAGES: 67
14. MONITORING AGENCY NAME & ADDRESS *(if different from Controlling Office)*: OklaMNE-78-2	15. SECURITY CLASS. *(of this report)*: unclassified 15a. DECLASSIFICATION/DOWNGRADING SCHEDULE

16. DISTRIBUTION STATEMENT *(of this Report)*

Approved for public release; distribution unlimited.

DISTRIBUTION STATEMENT A
Approved for public release;
Distribution Unlimited

17. DISTRIBUTION STATEMENT *(of the abstract entered in Block 20, if different from Report)*

18. SUPPLEMENTARY NOTES

19. KEY WORDS *(Continue on reverse side if necessary and identify by block number)*

20. ABSTRACT *(Continue on reverse side if necessary and identify by block number)*

An approximate analytical solution is obtained for hypersonic flow past a slender elliptic cone at small angle of attack. The analysis is based on perturbations of hypersonic flow past a circular cone aligned with the free stream, the perturbations stemming from the linear combination of small angle of attack and small cross-section eccentricity. By means of previously obtained hypersonic approximations for the basic-cone problem, closed-form approximate solutions for the perturbation equations are obtained within the framework of hypersonic small

DD FORM 1 JAN 73 1473 EDITION OF 1 NOV 65 IS OBSOLETE

UNCLASSIFIED
SECURITY CLASSIFICATION OF THIS PAGE *(When Data Entered)*

400 478

disturbance theory. Results for the shock shape, shock-layer structure, and surface conditions are presented, together with comparisons with experimental data.